

# IMPACT OF NEUTRINO FLAVOR OSCILLATIONS ON THE NEUTRINO-DRIVEN WIND NUCLEOSYNTHESIS OF AN ELECTRON-CAPTURE SUPERNOVA

ELSE PLLUMBI<sup>1,2</sup>, IRENE TAMBORRA<sup>3</sup>, SHINYA WANAJO<sup>4</sup>, HANS-THOMAS JANKA<sup>1</sup>, AND LORENZ HÜDEPOHL<sup>1</sup>

*Draft version June 12, 2014*

## ABSTRACT

Neutrino oscillations, especially to light sterile states, can affect the nucleosynthesis yields because of their possible feedback effect on the electron fraction ( $Y_e$ ). For the first time, we perform nucleosynthesis calculations for neutrino-driven wind trajectories from the neutrino-cooling phase of an  $8.8 M_\odot$  electron-capture supernova, whose hydrodynamic evolution was computed in spherical symmetry with sophisticated neutrino transport and whose  $Y_e$  evolution was post-processed by including neutrino oscillations both between active and active-sterile flavors. We also take into account the  $\alpha$ -effect as well as weak magnetism and recoil corrections in the neutrino absorption and emission processes. We observe effects on the  $Y_e$  evolution which depend in a subtle way on the relative radial positions of the sterile MSW resonances, of collective flavor transformations, and on the formation of  $\alpha$ -particles. For the adopted supernova progenitor, we find that neutrino oscillations, also to a sterile state with eV-mass, do not significantly affect the element formation and in particular cannot make the post-explosion wind outflow neutron rich enough to activate a strong r-process. Our conclusions become even more robust when, in order to mimic equation-of-state dependent corrections due to nucleon potential effects in the dense-medium neutrino opacities, four cases with reduced  $Y_e$  in the wind are considered. In these cases, despite the conversion of neutrinos to sterile neutrinos,  $Y_e$  increases compared to the values obtained without oscillations and active flavor transformations. This is a consequence of a complicated interplay between sterile-neutrino production, neutrino-neutrino interactions, and  $\alpha$ -effect.

*Subject headings:* supernovae: general — nuclear reactions, nucleosynthesis, abundances — neutrinos

## 1. INTRODUCTION

Stars with masses larger than  $\sim 8 M_\odot$  end their lives as core-collapse supernovae (CCSNe, e.g., Woosley et al. 2002). In particular, those with initial masses between  $\sim 8$  and  $\sim 10 M_\odot$  form electron-degenerate cores composed of oxygen, neon, and magnesium (O-Ne-Mg) and end their lives either as O-Ne-Mg white dwarfs or as “electron-capture supernovae” (ECSNe, Nomoto 1987) when electrons are captured on Ne and Mg and trigger the collapse of the stellar core. Since ECSNe represent up to 30% of all CCSNe (Ishimaru & Wanajo 1999; Poelarends et al. 2008; Wanajo et al. 2011b), they could significantly contribute to the Galactic chemical enrichment with heavy elements (Ishimaru & Wanajo 1999). Electron-capture supernovae were suggested as the site of r-process (rapid neutron-capture) element production (Hillebrandt et al. 1984; Wanajo et al. 2003; Ning et al. 2007). For comprehensive reviews on the r-process, see Wanajo & Ishimaru (2006); Arnould et al. (2007); Thielemann et al. (2011). However, recent nucleosynthesis studies (Hoffman et al. 2008; Wanajo et al. 2009), based on self-consistent hydrodynamic simulations of the explosion (Kitaura et al. 2006; Janka et al. 2008), do not support the production of elements with mass numbers heavier than  $A \sim 110$  in the early ejecta of ECSNe, but suggest interesting production of light trans-iron elements from Zn to Zr (Wanajo et al. 2011b), of  $^{48}\text{Ca}$  (Wanajo et al. 2013a)

and of  $^{60}\text{Fe}$  (Wanajo et al. 2013b). The two-dimensional hydrodynamic simulations do not provide conditions for a strong r-process, although a weak r-process cannot be excluded if the ejecta were slightly more neutron-rich than obtained in the models.

After the launch of the SN explosion, the proto-neutron star (PNS) cools because of the emission of neutrinos. Due to capture reactions and scattering events, neutrinos deposit energy in the outer layers of the PNS, giving birth to an outflow mainly composed of free neutrons and protons, the so-called neutrino-driven ( $\nu$ -driven) wind – see Janka (2012) and Arcones & Thielemann (2013) for recent reviews on the topic. While expanding away from the neutron star, the  $\nu$ -driven wind matter cools and the nucleons recombine, producing alpha particles and some fraction heavier nuclei. The  $\nu$ -driven wind has long been considered as a promising site of the r-process (Meyer et al. 1992; Woosley et al. 1994; Takahashi et al. 1994; Qian & Woosley 1996; Otsuki et al. 2000; Wanajo et al. 2001; Thompson et al. 2001). However, the outcome of the  $\nu$ -driven wind nucleosynthesis is strongly sensitive to the electron fraction  $Y_e$  (number of protons per nucleon), the entropy and the expansion timescale. Recent long-time hydrodynamic SN simulations with elaborate neutrino transport (Fischer et al. 2010; Hudepohl et al. 2010) show, besides insufficient entropy, a trend towards proton-rich  $\nu$ -driven winds, rather than neutron-rich ones as it would be required for an r-process to occur. Such proton-rich conditions might be suitable for the  $\nu p$ -process making some light  $p$ -nuclei (Fröhlich et al. 2006a,b; Pruet et al. 2006; Wanajo 2006).

More recently, however, it has been pointed out that the mean-field shift of nucleon potential energies (Reddy et al. 1998) significantly alters the charged-current neutrino opacity in the neutrinospheric layer and reduces  $Y_e$  from ini-

<sup>1</sup> Max-Planck-Institut für Astrophysik, Karl-Schwarzschild-Str. 1, D-85748 Garching, Germany; e-mail: epllumbi@mpa-garching.mpg.de, thj@mpa-garching.mpg.de, lorenz@mpa-garching.mpg.de

<sup>2</sup> Physik Department, Technische Universität München, James-Frank-Straße 1, 85748 Garching, Germany

<sup>3</sup> GRAPPA Institute, University of Amsterdam, Science Park 904, 1098 XH Amsterdam, The Netherlands; i.tamborra@uva.nl

<sup>4</sup> iTHES Research Group, RIKEN, Wako, Saitama 351-0198, Japan; e-mail: shinya.wanajo@riken.jp

tially proton-rich values down to possibly  $\sim 0.42\text{--}0.45$  for some temporary phase of the wind evolution (Roberts 2012; Martínez-Pinedo et al. 2012; Roberts et al. 2012). This effect was not adequately included in previous simulations, and it becomes important only when the neutrinosphere reaches high densities (postbounce time  $t_{\text{pb}} >$  a few 100 ms). At very late times, however, high neutrinospheric densities suppress  $\nu_e$  absorption on neutrons by final-state Pauli blocking of electrons (Fischer et al. 2012),  $\nu_e$  escape with harder spectra, and  $Y_e$  in the wind increases again. The matter at early and probably late times is thus still expected to be proton-rich.

One has to wonder whether favorable conditions for the r-process can still occur in supernovae. Since  $Y_e$  depends on the competition between the capture rates of  $\nu_e$  and  $\bar{\nu}_e$  on free nucleons and their inverse reactions (Fuller & Meyer 1995), a modification of the predicted neutrino energy spectra, for example due to nucleon-potential effects, can affect  $Y_e$  in the neutrino-driven outflows. Also neutrino oscillations could modify the wind- $Y_e$ , if they significantly alter the  $\nu_e$  and  $\bar{\nu}_e$  fluxes before  $Y_e$  reaches its asymptotic value. Therefore, the inclusion of flavor oscillations may be crucial for determining the nuclear production in the  $\nu$ -driven wind matter and to clarify whether ECSNe could still be considered as candidate sites for the r-process.

The nucleosynthesis yields (and the r-process) in supernovae might be affected by the existence of light sterile neutrinos, hypothetical gauge-singlet fermions that could mix with one or more of the active states and thus show up in active-sterile flavor oscillations (see Abazajian et al. 2012; Palazzo 2013 for recent reviews on the topic). In particular, eV-mass sterile neutrinos with large mixing imply that the  $\nu_e$  flux would undergo Mikheyev-Smirnov-Wolfenstein (MSW) conversions (Mikheyev & Smirnov 1985; Wolfenstein 1978) to  $\nu_s$  closer to the SN core than any other oscillation effect. We assume that the sterile state is heavier than the active ones because of cosmological neutrino mass limits (Abazajian et al. 2012). The idea that removing the  $\nu_e$  flux by active-sterile oscillations could favor a neutron-rich outflow environment was proposed some time ago (Beun et al. 2006; Keränen et al. 2007; Fetter et al. 2003; Fetter 2000; McLaughlin et al. 1999; Hidaka & Fuller 2007; Nunokawa et al. 1997). However, the considered mass differences were larger and the possible impact of  $\nu$ - $\nu$  interactions in the active sector (Duan et al. 2010) was not taken into account.

Recently, renewed interest for low-mass sterile neutrinos has arisen since they have been invoked to explain the excess  $\bar{\nu}_e$  events in the LSND experiment (Aguilar et al. 2001; Strumia 2002; Gonzalez-Garcia & Maltoni 2008) as well as the MiniBooNE excess (Aguilar-Arevalo et al. 2009a,b; Karagiorgi et al. 2009; MiniBooNE Collaboration et al. 2012). Moreover an indication for the possible existence of eV-mass sterile neutrinos comes from a new analysis of reactor  $\bar{\nu}_e$  spectra and short-baseline experiments (Kopp et al. 2011; Giunti & Laveder 2011a,b; Giunti et al. 2012; Donini et al. 2012; Giunti et al. 2013). The cosmic microwave background anisotropies (Reid et al. 2010; Hamann et al. 2010; Hou et al. 2013; Hinshaw et al. 2013; Planck Collaboration et al. 2013; Archidiacono et al. 2013) as well as big-bang nucleosynthesis (Pettini & Cooke 2012; Aver et al. 2012) point towards a cosmic excess radiation compatible with one family of fully thermalized sub-eV sterile neutrinos or one or even two partially thermalized sterile neutrino families with sub-eV/eV mass (Archidiacono et al. 2013; Giusarma et al. 2014).

Such intense activity triggered new interest in the role of neutrino oscillations with and without sterile neutrinos, and including  $\nu$ - $\nu$  interactions, on nucleosynthesis processes like the r-process and the  $\nu p$ -process in SN outflows (Tamborra et al. 2012b; Duan et al. 2011; Martínez-Pinedo et al. 2011). The role of active-sterile neutrino mixing for the  $\nu$ -driven explosion mechanism and the nucleosynthesis in the early ( $t \leq 100$  ms postbounce) ejecta of ECSNe was discussed by Wu et al. (2014). The authors found that active-sterile conversions can not only suppress neutrino heating considerably but can potentially enhance the neutron-richness of the ejecta allowing for the production of the elements from Sr, Y and Zr up to Cd. The conclusiveness of these results is unclear, however, because, besides approximate modeling of neutrino oscillations, only spherically symmetric models were considered, although multi-dimensional effects had been shown to be important during the onset of the explosion (cf. Wanajo et al. 2011b). In contrast to spherical models, multi-dimensional ones provide sufficient neutron excess to yield interesting amounts of elements between the Fe-group and  $N = 50$  nuclei even without involving sterile neutrino effects Wanajo et al. (2011b).

In this work, we explore the impact of neutrino flavor oscillations (with and without the inclusion of an extra eV-mass sterile neutrino) on the  $Y_e$  evolution of the  $\nu$ -driven wind and on the corresponding nucleosynthesis yields of an ECSN, whose evolution can be well described in spherical symmetry and has been followed beyond the explosion continuously into the subsequent proto-neutron star cooling phase (Hüdepohl et al. 2010). The simulation of Hüdepohl et al. (2010) did not include the aforementioned nucleon mean-field effects in the charged-current neutrino-nucleon reactions and resulted in the ejection of proton-rich matter throughout the wind phase. We still use this model to examine neutrino oscillation effects in the neutrino-driven wind, because the wind dynamics and thermodynamics conditions are only marginally changed despite the impact of the nucleon potentials on the electron fraction (e.g. Martínez-Pinedo et al. 2012).

Our paper is structured in the following way. In Sect. 2, we describe the  $\nu$ -driven wind trajectories adopted for the nucleosynthesis calculations, as well as our reaction network. In Sect. 3, the electron fraction evolution and the nucleosynthesis results are presented when no neutrino oscillations occur as fiducial case. After introducing the neutrino mass-mixing parameters in Sect. 4, we briefly discuss the oscillation physics involved in the nucleosynthesis calculations. Our results for  $Y_e$  and how it is affected by neutrino oscillations (with and without sterile neutrinos) including the corresponding nucleosynthesis are presented in Sect. 5. In Sect. 6, we introduce four toy model cases for the  $\nu_e$  and  $\bar{\nu}_e$  energy spectra in order to explore the possible consequences of nuclear mean-field effects in the neutrino opacities. Finally, we present our conclusions and perspectives in Sect. 7.

## 2. NEUTRINO-DRIVEN WIND AND REACTION NETWORK

We use one-dimensional (1D) long-time simulations of a representative  $8.8 M_{\odot}$  progenitor (Hüdepohl et al. 2010), performed with the equation of state of Shen et al. (1998). For the present study we adopt the Model Sf 21 (see Hüdepohl et al. 2010 for further details<sup>5</sup>). In the cho-

<sup>5</sup> Model Sf 21 is analog to model Sf of Hüdepohl et al. (2010) but was computed with 21 energy bins for the neutrino transport instead of the usual

sen model, the accretion phase ends already at a postbounce time of  $t_{\text{pb}} \sim 0.2$  s when neutrino heating drives the expansion of the postshock layers and powers the explosion. The subsequent deleptonization and cooling of the PNS were followed for  $\sim 10$  s.

In order to perform the network calculations for the nucleosynthesis in the neutrino-driven wind, we use 98 ejecta trajectories. Figure 1 shows the time evolution of the distance  $r$  from the center of the PNS (top panel), temperature  $T$  (middle panel), and matter density  $\rho$  (bottom panel) for these mass-shell trajectories as functions of  $t_{\text{pb}}$ . The outflow evolution of 7 of the 98 trajectories, corresponding to initial times  $t_0 = 0.5, 1, 2, 2.9, 4.5, 6.5, 7.5$  s ( $t_0$  being measured when the temperature  $T_0 = 9$  GK), is highlighted with different colors. We adopt these seven trajectories as representative of the cooling evolution of the PNS to discuss the impact of neutrino oscillations (with and without an additional light sterile neutrino) on the nucleosynthesis in the  $\nu$ -driven wind. The total ejecta mass of the 98 mass-shell trajectories is  $M_{98} = 1.1 \times 10^{-2} M_{\odot}$ .

In the network, 6300 species are included between the proton-drip line and neutron-drip line, up to the  $Z = 110$  isotopes (see Wanajo et al. 2009, for more details). All the important reactions such as  $\nu_e(n, p)e^-$ ,  $\bar{\nu}_e(p, n)e^+$ ,  $(n, \gamma)$ ,  $(p, \gamma)$ ,  $(\alpha, \gamma)$ ,  $(p, n)$ ,  $(\alpha, n)$ ,  $(\alpha, p)$ , and their inverse ones are taken into account. The  $\nu_e$  and  $\bar{\nu}_e$  capture rates on free neutrons and protons are calculated as in Horowitz & Li (1999) and thus include recoil and weak magnetism corrections. The neutrino-induced reactions on heavy nuclei are not included since they have negligible effects (Meyer et al. 1998). The nucleosynthesis calculations start when the mass-shell temperature decreases to 9 GK, with an initial composition of free neutrons and protons with number fractions of  $1 - Y_e$  and  $Y_e$ , respectively.

### 3. ELECTRON FRACTION EVOLUTION

The matter in a fluid element moving away from the PNS will experience three stages of nuclear evolution. Near the surface of the PNS, the temperature is so high that the matter is in nuclear statistical equilibrium (NSE) and nearly all of the baryons are in the form of free nucleons. As the material flows away from the PNS, it cools. When the temperature is  $T < 1$  MeV,  $\alpha$  particles begin to assemble, from which heavier nuclei form by  $\alpha\alpha n$  and  $3\alpha$  reactions and subsequent captures of  $\alpha$  particles and free nucleons.

Together with the entropy and the expansion time, a basic quantity defining the conditions for element formation (and eventually an r-process) is the excess of initially free  $n$  or  $p$  expressed by the electron fraction  $Y_e$ . It is locally defined as the ratio of the net electron (electrons minus positrons) number density,  $N_e$ , to the sum of proton number density  $N_p$  and neutron number density  $N_n$ :

$$Y_e(r) = \frac{N_e(r)}{N_p(r) + N_n(r)} = X_p(r) + \frac{X_{\alpha}(r)}{2} + \sum_{Z_A > 2} \frac{Z_A(r)}{A(r)} X_A(r), \quad (1)$$

where  $X_p$ ,  $X_{\alpha}$ , and  $X_A$  are the mass fractions of free protons ( $p$ ),  $\alpha$  particles, and heavy elements ( $Z_A > 2$ ) as functions of the radius. The charge and the mass numbers of the heavy nuclear species are  $Z_A$  and  $A$ , respectively. In all neutral media,  $Y_e = Y_p$  and  $Y_n = 1 - Y_e$ , with  $Y_j$  being the

17 energy groups.

number density of free or bound particle species  $j$  relative to baryons. The lower  $Y_e$  is, the more the environment is neutron rich, and thus the more favorable it is for the r-process to occur (e.g. Hoffman et al. 1997). On the other hand,  $Y_e > 0.5$  implies that the matter is proton-rich and  $p$ -rich nuclei could be formed through the  $\nu p$ -process (Fröhlich et al. 2006a; Pruet et al. 2006; Wanajo 2006).

Having in mind the overall evolution of abundances with radius and time and assuming that the reactions of neutrinos on nuclei are negligible, the  $n/p$  ratio in the wind ejecta is set by  $\beta$ -interactions of electron neutrinos ( $\nu_e$ ) and electron antineutrinos ( $\bar{\nu}_e$ ) with free  $n$  and  $p$  and their inverse reactions:

$$\nu_e + n \rightleftharpoons p + e^-, \quad (2)$$

$$\bar{\nu}_e + p \rightleftharpoons n + e^+. \quad (3)$$

The  $Y_e$  evolution therefore depends on the spectra and luminosities of  $\nu_e$  and  $\bar{\nu}_e$ . Modifications of the neutrino emission properties, such as the energy spectra, due to flavor oscillations could significantly change the  $n/p$  ratio and thus  $Y_e$  in the wind.

Because of slow time variations of the outflow conditions during the PNS cooling phase, a near steady-state situation applies (Qian & Woosley 1996) and the rate-of-change of  $Y_e$  within an outflowing mass element can be written as in McLaughlin et al. (1996):

$$\frac{dY_e}{dt} = v(r) \frac{dY_e}{dr} \simeq (\lambda_{\nu_e} + \lambda_{e^+}) Y_n^f - (\lambda_{\bar{\nu}_e} + \lambda_{e^-}) Y_p^f, \quad (4)$$

where  $v(r)$  is the velocity of the outflowing mass element, the  $\lambda_i$  are the reaction rates, and  $Y_n^f$  and  $Y_p^f$  are the abundances of free nucleons.

In the free streaming limit with neutrinos propagating radially, the forward reaction rates of Eqs. (2,3) can be written in terms of the electron (anti)neutrino emission properties as:

$$\lambda_{\nu_e} \simeq \frac{L_{\nu_e}}{4\pi r^2 \langle E_{\nu_e} \rangle} \langle \sigma_{\nu_e} \rangle, \quad (5)$$

$$\lambda_{\bar{\nu}_e} \simeq \frac{L_{\bar{\nu}_e}}{4\pi r^2 \langle E_{\bar{\nu}_e} \rangle} \langle \sigma_{\bar{\nu}_e} \rangle, \quad (6)$$

where  $L_{\nu_e}$  and  $L_{\bar{\nu}_e}$  are the luminosities of  $\nu_e$  and  $\bar{\nu}_e$  respectively,  $\langle E_{\nu_e} \rangle$  and  $\langle E_{\bar{\nu}_e} \rangle$  the mean spectral energies<sup>6</sup>. The  $\nu_e$  and  $\bar{\nu}_e$  capture cross sections of the forward reactions (2,3), averaged over the corresponding  $\nu_e$  and  $\bar{\nu}_e$  energy spectra, are  $\langle \sigma_{\nu_e} \rangle$  and  $\langle \sigma_{\bar{\nu}_e} \rangle$ , respectively. Including the weak magnetism and recoil corrections, the average neutrino capture cross sections are (Horowitz & Li 1999):

$$\langle \sigma_{\nu_e} \rangle \simeq k \langle E_{\nu_e} \rangle \varepsilon_{\nu_e} \left[ 1 + 2 \frac{\Delta}{\varepsilon_{\nu_e}} + a_{\nu_e} \left( \frac{\Delta}{\varepsilon_{\nu_e}} \right)^2 \right] W_{\nu_e}, \quad (7)$$

$$\langle \sigma_{\bar{\nu}_e} \rangle \simeq k \langle E_{\bar{\nu}_e} \rangle \varepsilon_{\bar{\nu}_e} \left[ 1 - 2 \frac{\Delta}{\varepsilon_{\bar{\nu}_e}} + a_{\bar{\nu}_e} \left( \frac{\Delta}{\varepsilon_{\bar{\nu}_e}} \right)^2 \right] W_{\bar{\nu}_e}, \quad (8)$$

where  $k \simeq 9.3 \cdot 10^{-44} \text{ cm}^2/\text{MeV}^2$ ,  $\varepsilon_{\nu} = \langle E_{\nu}^2 \rangle / \langle E_{\nu} \rangle$  ( $\nu = \nu_e, \bar{\nu}_e$ ),  $a_{\nu} = \langle E_{\nu}^2 \rangle / \langle E_{\nu} \rangle^2$ ,  $M$  is the nucleon mass in MeV and  $\Delta = 1.293$  MeV is the neutron-proton mass difference. The weak magnetism and recoil correction factors are given by  $W_{\nu_e} = [1 + 1.02 b_{\nu_e} \varepsilon_{\nu_e} / M]$  and  $W_{\bar{\nu}_e} = [1 - 7.22 b_{\bar{\nu}_e} \varepsilon_{\bar{\nu}_e} / M]$ , where  $b_{\nu} =$

<sup>6</sup>  $\langle E_{\nu}^n \rangle \equiv \int E_{\nu}^n f(E_{\nu}) dE$ , where  $f(E_{\nu})$  is the normalized (anti)neutrino energy spectrum. The energy spectrum which we use will be described in Sect. 4.

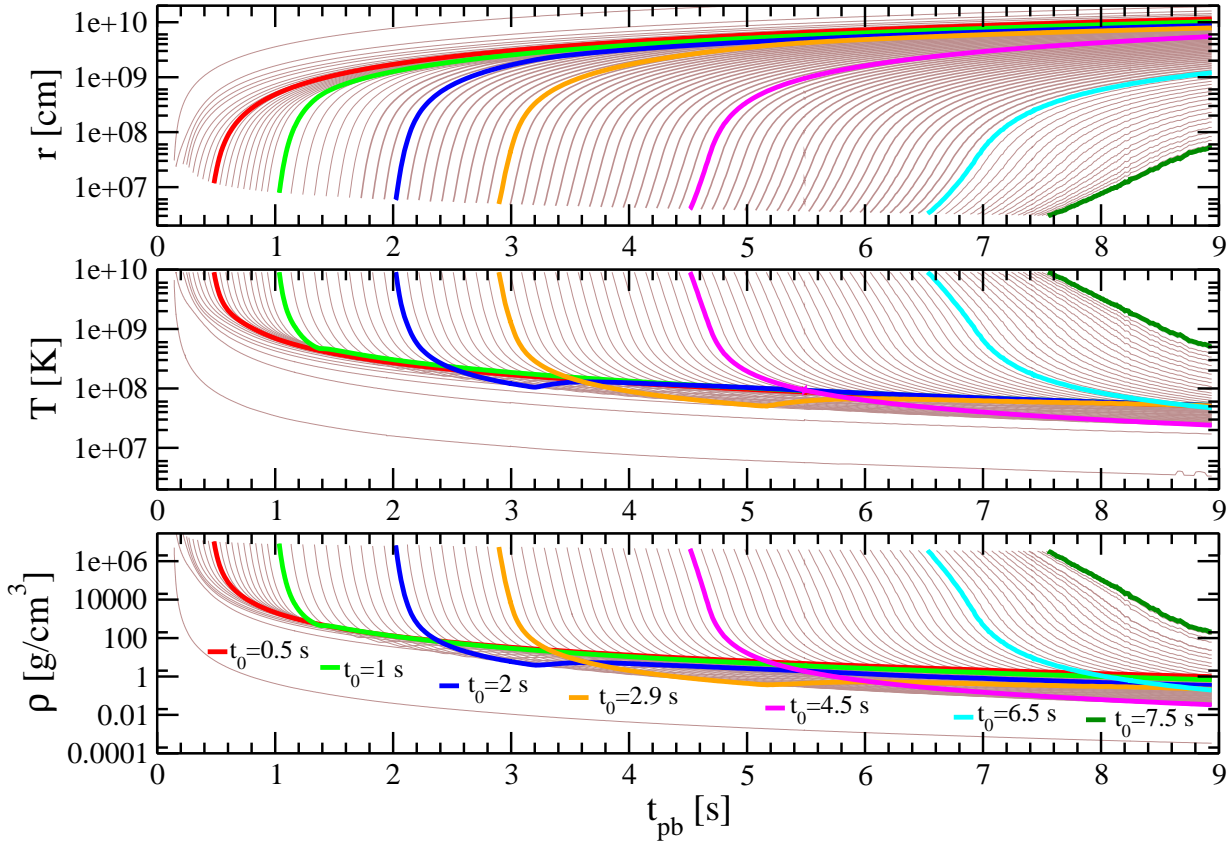


FIG. 1.— Mass-shell trajectories of the neutrino-driven wind as functions of postbounce time ( $t_{\text{pb}}$ ): Radial distance from the PNS center (top), temperature (middle), and density (bottom) along the ejecta trajectories. The colored curves correspond to the selected 7 trajectories representative of the evolution of the  $\nu$ -driven wind for initial times,  $t_0 = 0.5, 1, 2, 2.9, 4.5, 6.5, 7.5$  s. The kinks visible in the temperature and density evolutions of the trajectories for  $t_0 = 2$  s and 2.9 s indicate the existence of a weak reverse shock.

$\langle E_\nu^3 \rangle \langle E_\nu \rangle / \langle E_\nu^2 \rangle^2$  represents the spectral shape factor for  $\nu_e$  or  $\bar{\nu}_e$ . We point out that in Eq. (8) the spectral integration was approximated by integrating over the interval  $[0, \infty)$  instead of  $[\Delta, \infty)$ . Since the rates  $\lambda_{\nu_e}$  and  $\lambda_{\bar{\nu}_e}$  are functions of the neutrino fluxes, they can be affected by neutrino flavor conversions.

The inverse reaction rates  $\lambda_{e^-}$  and  $\lambda_{e^+}$  of reactions (2,3), are given, in analogy to the forward reaction rates, by:

$$\lambda_{e^-} = c \cdot \tilde{n}_{e^-} \cdot \langle \sigma_{e^-} \rangle, \quad (9)$$

$$\lambda_{e^+} = c \cdot n_{e^+} \cdot \langle \sigma_{e^+} \rangle, \quad (10)$$

where  $c$  is the speed of light. In Eq. (9),  $\tilde{n}_{e^-}$  is slightly modified compared to the electron number density and given by:

$$\tilde{n}_{e^-} = \frac{8\pi}{(2\pi\hbar c)^3} \cdot \int_0^\infty \frac{\epsilon^2}{1 + \exp[\frac{\epsilon - \tilde{\mu}_e}{k_B T}]} d\epsilon, \quad (11)$$

where  $\tilde{\mu}_e = \mu_e - \Delta$  and  $\mu_e$  is the electron chemical potential. The average cross section  $\langle \sigma_{e^-} \rangle$  of the inverse reaction (2) is:

$$\langle \sigma_{e^-} \rangle \simeq \frac{1}{2} k \langle \tilde{E}_{e^-} \rangle \epsilon_{e^-} \left[ 1 + 2 \frac{\Delta}{\epsilon_{e^-}} + a_{e^-} \left( \frac{\Delta}{\epsilon_{e^-}} \right)^2 \right] W_{\nu_e}, \quad (12)$$

where  $\epsilon_{e^-} = \langle \tilde{E}_{e^-}^2 \rangle / \langle \tilde{E}_{e^-} \rangle$  and  $a_{e^-} = \langle \tilde{E}_{e^-}^3 \rangle / \langle \tilde{E}_{e^-} \rangle^2$ . In analogy to  $\langle E_\nu^n \rangle$ ,  $\langle \tilde{E}_{e^-}^n \rangle$  is defined by using  $\tilde{f}_{e^-}(E) = \frac{\tilde{\xi}_{e^-} E^2}{1 + \exp[(E - \tilde{\mu}_e)/k_B T]}$  for the electron distribution function with  $\tilde{\xi}$  being the normalization factor such that  $\int \tilde{f}_{e^-}(E) dE = 1$ . In Eq. (10), the positron

number density is given by:

$$n_{e^+} = \frac{8\pi}{(2\pi\hbar c)^3} \cdot \int_0^\infty \frac{\epsilon^2}{1 + \exp[\frac{\epsilon + \mu_e}{k_B T}]} d\epsilon, \quad (13)$$

and the positron average capture cross section is given by:

$$\langle \sigma_{e^+} \rangle \simeq \frac{1}{2} k \langle E_{e^+} \rangle \epsilon_{e^+} \left[ 1 + 2 \frac{\Delta}{\epsilon_{e^+}} + a_{e^+} \left( \frac{\Delta}{\epsilon_{e^+}} \right)^2 \right] W_{\bar{\nu}_e}, \quad (14)$$

where  $\epsilon_{e^+} = \langle E_{e^+}^2 \rangle / \langle E_{e^+} \rangle$  and  $a_{e^+} = \langle E_{e^+}^3 \rangle / \langle E_{e^+} \rangle^2$ . The energy moments are calculated using the positron distribution function  $f_{e^+}(E) = \frac{\xi_{e^+} E^2}{1 + \exp[(E - \mu_e)/k_B T]}$ , where  $\xi_{e^+}$  is the normalization factor such that  $\int f_{e^+}(E) dE = 1$ .

We approximate the weak magnetism and recoil corrections in Eqs. (12,14) by using  $W_{\nu_e}$  and  $W_{\bar{\nu}_e}$  of Eqs. (7,8) with the energy moments of the emitted neutrinos, fulfilling the detailed balance theorem. We notice that in Eqs. (12,14) and Eqs. (7,8) we have neglected the mass of the electron,  $m_e$ , since it does not make any difference in our calculations ( $m_e \ll E \pm \Delta$ ). We also point out that  $\lambda_{e^-}$  and  $\lambda_{e^+}$ , neglecting weak magnetism and recoil corrections (i.e. for  $W_{\nu_e} = W_{\bar{\nu}_e} = 1$ ), but including  $m_e$ -dependent terms, are given in Bruenn (1985).

The nucleons involved in the  $\beta$ -reactions of Eq. (4) are free. Accounting for the nucleons bound in  $\alpha$  particles, the number fractions of free protons and neutrons can be written as

functions of  $Y_e$  as:

$$Y_p^f = Y_e - \frac{X_\alpha}{2} - \sum_{Z_A > 2} \frac{Z_A}{A} X_A, \quad (15)$$

$$Y_n^f = 1 - Y_e - \frac{X_\alpha}{2} - \sum_{Z_A > 2} \frac{N_A}{A} X_A, \quad (16)$$

where  $X_\alpha$  ( $X_A$ ) is the mass fraction of  $\alpha$  particles (heavy nuclei). In Table 1, we list the  $Y_e$  values at the neutrinosphere<sup>7</sup> radius  $R_\nu$  for the selected seven postbounce times  $t_0$ , as obtained from the numerical simulation of Model Sf 21 of H\"udepohl et al. (2010).

Since we aim at discussing the role of neutrino oscillations and of the so-called “ $\alpha$ -effect” on the  $Y_e$  and nucleosynthesis in the  $\nu$ -driven wind, we distinguish two cases with different  $X_\alpha$  in what follows:

- (i) We compute  $X_\alpha$  using the full network (labelled “incl.  $\alpha$ -effect”);
- (ii) We keep  $X_\alpha$  constant at its value at  $T = 9$  GK as given by Model Sf 21.

The recombination of free nucleons to  $\alpha$ -particles affects  $Y_p^f$  and  $Y_n^f$  according to Eqs. (15) and (16) and via Eq. (4) influences the evolution of  $Y_e$ . Since the formation of  $\alpha$ -particles binds equal numbers of neutrons and protons, the remaining free nucleons will be dominated by the more abundant nucleonic species, either  $n$  or  $p$ . The corresponding capture reactions of  $\nu_e$  (and  $e^+$ ) on neutrons in the case of neutron excess or of  $\bar{\nu}_e$  (and  $e^-$ ) on protons for proton-rich conditions will drive  $Y_e$  closer to 0.5, which is the so-called  $\alpha$ -effect first pointed out by McLaughlin et al. (1996) and Meyer et al. (1998). Assuming  $X_\alpha$  to remain constant in case (ii) for  $T < 9$  GK allows us to compare our results with Tamborra et al. (2012b), where this prescription was applied for simplicity in default of a network solver to follow the detailed evolution of the nuclear abundances when matter falls out of NSE. Furthermore, since a proper inclusion of the  $\alpha$ -effect always requires detailed network calculations as in our case (i), we consider case (ii) for isolating the effect of the formation of  $\alpha$  particles on  $Y_e$ , as we will elucidate in Sect. 5.

### 3.1. Nucleosynthesis yields without neutrino oscillations

In this section, we discuss as our fiducial case the results of nucleosynthesis in the  $\nu$ -driven wind ejecta of an  $8.8 M_\odot$  ECSN without taking into account neutrino oscillations (but including the  $\alpha$ -effect). Note that nucleosynthesis computations were done in previous papers adopting semi-analytically (Wanajo et al. 2001; Wanajo 2006) or hydrodynamically (Fr\"ohlich et al. 2006b; Takahashi et al. 1994; Pruet et al. 2006; Arcones & Montes 2011) computed neutrino-driven winds. With the exception of investigations by Meyer et al. (1992) and Woosley et al. (1994), who used the now outdated model of J. Wilson, however, the other existing calculations were based on a number of simplifications or considered only constrained periods of evolution (like Pruet et al. 2006). In this sense, our study is the first

one in which the wind nucleosynthesis is explored in a self-consistently exploded progenitor, whose evolution was continuously followed from collapse to beyond the explosion through the complete subsequent proto-neutron star cooling phase. Nevertheless, the results should not be taken as firm nucleosynthetic prediction to be used for galactic chemical evolution studies because of the absence of dense-medium nucleon potential effects in the charged-current neutrino reactions of the hydrodynamic simulation. The inclusion of these nucleon-potential effects will cause nuclear equation-of-state dependent modifications of the neutrino emission and therefore of the  $Y_e$  evolution in the  $\nu$ -driven wind (e.g. Mart\'inez-Pinedo et al. 2012; Roberts 2012; Roberts et al. 2012), whose investigation is beyond the present work.

Including 98 trajectories,  $X_A$  is given by:

$$X_A = \frac{1}{M_{\text{tot}}} \sum_{i=1}^{98} X_{i,A} \Delta M_i, \quad (17)$$

where  $X_{i,A}$  and  $\Delta M_i$  are the mass fractions and the ejecta-shell masses respectively, while  $M_{\text{tot}}$  is the total mass of the ejecta, which we consider to be the sum of the ejected mass from the core plus the outer H/He-envelope (assumed to contain no heavy elements):

$$M_{\text{tot}} = (8.8 M_\odot - 1.366 M_\odot) + 0.0114 M_\odot \approx 7.44 M_\odot.$$

Here  $1.366 M_\odot$  defines the initial mass cut between neutron star and ejecta. In order to discuss the impact of neutrino oscillations<sup>8</sup> in the following sections, we replace the full set of 98 trajectories by 7 “representative”  $\nu$ -driven wind trajectories (Fig. 1).

For the 7 representative wind trajectories, we define combined mass elements,  $\Delta \bar{M}_j$  ( $j = 1, \dots, 7$ ), in such a way that  $\Delta \bar{M}_j = \sum_{i=i_{j-1}+1}^{i_j} \Delta M_i$ , where the summation includes all mass shells ejected between the representative shell  $i_{j-1}$  and the representative shell  $i_j$  (see Table 1). The first representative shell, for example, includes all the 10 trajectories of the full set which are ejected before  $t_0 = 0.5$  s. Thus, for the 7 representative trajectories, we define:

$$\bar{X}_A = \frac{1}{M_{\text{tot}}} \sum_{j=1}^7 X_{j,A} \Delta \bar{M}_j, \quad (18)$$

with  $X_j$  being the mass fractions for the  $j$ -th trajectory.

Figure 2 shows the nucleosynthesis mass fractions, without taking into account neutrino oscillations, for the 98 trajectories and for the 7 trajectories after mass integration over the ejecta mass-shell range as given by Eqs. (17) and (18), respectively. In the left panel, the mass fractions  $X_A$  obtained for all of the 98 available  $\nu$ -driven wind trajectories are compared to the ones obtained for the 7 selected trajectories. In the right panel of Fig. 2, the isotopic mass fractions  $X_A$  relative to the solar ones  $X_\odot$  (Lodders 2003, i.e. the production factors) are shown for the 98 available  $\nu$ -driven wind trajectories and for the 7 representative ones as functions of  $A$ . The dotted horizontal lines represent a “normalization band.” The isotopes which fall into this band are considered to be the main nucleosynthetic products from the neutrino-driven wind phase

<sup>7</sup> The neutrinosphere is defined as the region at which the neutrinos or antineutrinos escape from the proto-neutron star surface. We notice that, in general, the neutrinosphere  $R_\nu$  is different for different (anti)neutrino flavors. We assume  $R_\nu$  to be roughly the same for all flavors.

<sup>8</sup> We assume that the  $\nu_e$  and  $\bar{\nu}_e$  luminosities and energy spectra do not change for  $r \geq R_\nu$ . This means that we do not only ignore small evolutionary changes due to remaining neutrino interactions in the external medium but we also disregard general relativistic redshift corrections, which depend on  $r$ , and which are included in the hydrodynamic simulations.

TABLE 1  
NEUTRINOSPHERIC PARAMETERS AND ELECTRON FRACTIONS  $Y_e$  AS FUNCTIONS OF POSTBOUNCE TIME  $t_0$ .

$t_0^a$ [s]	$R_\nu^b$ [ $10^5$ cm]	$Y_e^c$	$Y_{e,a}^d$	$\Delta\bar{M}_j^e$ [ $10^{-3} M_\odot$ ]	$L_{\nu_e}^f$ [ $10^{51}$ erg/s]	$L_{\bar{\nu}_e}^g$ [ $10^{51}$ erg/s]	$L_{\nu_x}^h$ [ $10^{51}$ erg/s]	$\langle E_{\nu_e} \rangle^i$ [MeV]	$\langle E_{\bar{\nu}_e} \rangle^j$ [MeV]	$\langle E_{\nu_x} \rangle^k$ [MeV]	$\alpha_{\nu_e}^l$	$\alpha_{\bar{\nu}_e}^m$	$\alpha_{\nu_x}^n$
0.5	25.0	0.0547	0.554	9.640	9.5	10.10	10.80	16.8	18.1	18.3	2.9	3.0	2.8
1.0	20.5	0.0522	0.546	0.770	7.3	8.30	7.90	15.9	17.4	17.3	3.0	2.9	2.6
2.0	17.5	0.0445	0.564	0.380	4.7	4.90	5.30	15.3	16.5	16.1	3.2	2.7	2.3
2.9	16.0	0.0323	0.566	0.110	3.3	3.40	3.70	15.8	16.3	15.7	3.1	2.3	2.5
4.5	15.2	0.0268	0.574	0.060	1.9	1.90	2.00	13.8	13.4	12.9	3.0	2.3	2.1
6.5	14.5	0.0233	0.555	0.020	1.0	0.99	1.04	12.4	11.9	11.8	2.6	2.3	2.4
7.5	14.5	0.0223	0.549	0.002	0.6	0.60	0.60	9.9	9.6	9.5	2.4	2.3	2.5

<sup>a</sup> Postbounce time.

<sup>b</sup> Neutrinosphere radius.

<sup>c</sup> Electron fraction at  $R_\nu$ .

<sup>d</sup> Asymptotic electron fraction (at  $r = 3 \cdot 10^7$  cm).

<sup>e</sup>  $\Delta\bar{M}_j$ : ejecta mass of the 7 representative wind trajectories.

<sup>f, g, h</sup> Luminosities of  $\nu_e$ ,  $\bar{\nu}_e$  and  $\nu_x$ , respectively.

<sup>i, j, k</sup> Mean energies of  $\nu_e$ ,  $\bar{\nu}_e$  and  $\nu_x$ , respectively.

<sup>l, m, n</sup> Spectral fitting parameters of  $\nu_e$ ,  $\bar{\nu}_e$  and  $\nu_x$ , respectively (see Sect. 4).

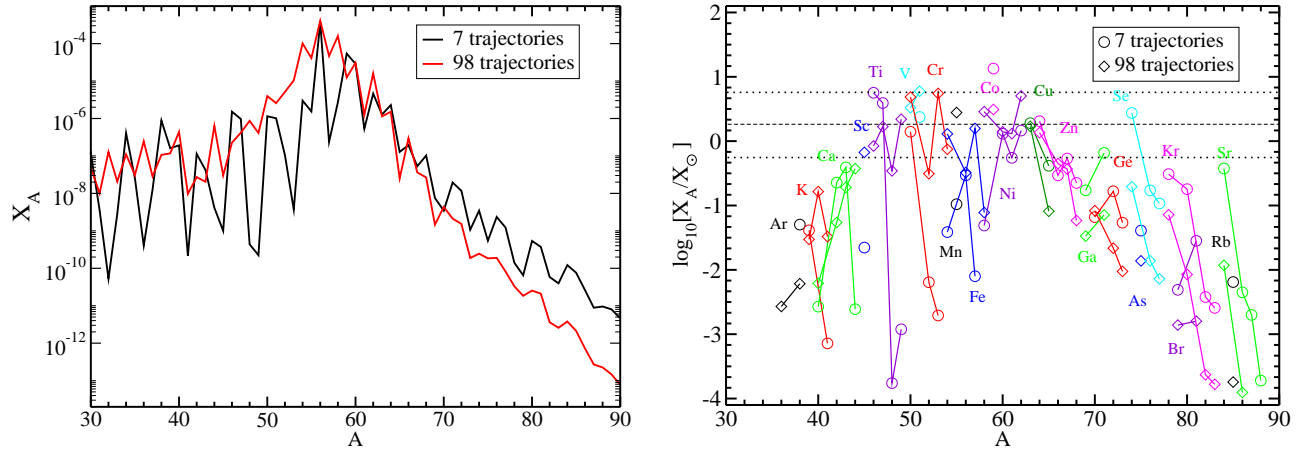


Fig. 2.— *Left*: Mass fractions  $X_A$  of the ejecta as a function of mass number  $A$  comparing the cases for 7 representative trajectories and for all the 98 trajectories. *Right*: Comparison of the isotopic ejecta mass fractions ( $X_A$ ) relative to the solar ones ( $X_\odot$ ). The horizontal upper dotted line passes through the most overproduced isotopes ( $^{51}\text{V}$ ,  $^{53}\text{Cr}$ , and  $^{62}\text{Ni}$ ) in the 98 trajectory case, and the horizontal lower dotted line lies a factor of ten below the level of the upper line. The dashed line represents the median value. Our 7 selected trajectories reproduce the case with the 98 trajectories satisfactorily well only for certain values of  $A$  (e.g.  $58 \leq A \leq 69$ ).

of our fiducial ECSN model that could contribute to galactic chemical evolution. The upper dotted line passes through the most overproduced elements ( $^{51}\text{V}$ ,  $^{53}\text{Cr}$ , and  $^{62}\text{Ni}$ ), and the lower dotted line lies a factor of ten below that. The middle dashed line represents the median value.

We find that the nucleosynthesis yields of the 7 trajectories, because of the coarse time resolution of the wind history, reproduce those obtained from all the 98 trajectories only very approximately. Nevertheless, this will be qualitatively sufficient to discuss the effects of neutrino oscillations on the nucleosynthesis conditions. The right panel of Fig. 2 shows little production of isotopes with  $A > 65$  in the 98 trajectory case as well as in the 7 trajectory case. This is a consequence of only a weak  $\nu p$ -process<sup>9</sup> in this supernova environment because of the absence of a dense outer stellar envelope in ECSNe, which is crucial for an efficient  $\nu p$ -process (Wanajo et al. 2011a). Many of the iron-group and light trans-iron isotopes still lie

on the normalization band, but the greatest production factors (for  $^{51}\text{V}$ ,  $^{53}\text{Cr}$ , and  $^{62}\text{Ni}$  in the 98 trajectory case) are below 10. For example, the production factor of  $^{62}\text{Ni}$  is several times smaller than the corresponding one in the early ( $\lesssim 400$  ms) convective ejecta, which are absent in 1D but found in the 2D counterpart of the ECSN explosion model (Wanajo et al. 2011b, 2013a). It appears, therefore, that the nucleosynthetic contribution of the  $\nu$ -driven wind to the Galactic chemical evolution is unimportant. It should be noted, however, that the effects of nucleon potential corrections might alter the  $Y_e$  history and thus the wind contribution could be more important for nucleosynthesis than found here.

#### 4. REFERENCE NEUTRINO SIGNAL AND FLAVOR EVOLUTION EQUATIONS

At radius  $r$  outside of the neutrinosphere, the unoscillated spectral number fluxes for each flavor  $\nu$  ( $\nu = \nu_e, \bar{\nu}_e, \nu_x, \bar{\nu}_x$  with  $x = \mu$  or  $\tau$ ) can be approximated by:

$$F_\nu(E) \approx \frac{L_\nu}{4\pi r^2} \frac{f_\nu(E)}{\langle E_\nu \rangle}, \quad (19)$$

<sup>9</sup> In Table 1, we show the asymptotic values (indicated by subscript “a”) of the electron fraction  $Y_{e,a}$  for our 7 representative trajectories. Notice that since  $Y_{e,a} > 0.5$  for all the considered cases, the  $\nu p$ -process may be enabled.

where  $L_\nu$  is the luminosity for the flavor  $\nu$  and  $\langle E_\nu \rangle$  the mean spectral energy<sup>10</sup>. The neutrino spectrum  $f_\nu(E)$  is well reproduced by a combined power-law and exponential fit (Keil et al. 2003; Tamborra et al. 2012a):

$$f_\nu(E) = \xi_\nu \left( \frac{E}{\langle E_\nu \rangle} \right)^{\alpha_\nu} e^{-(\alpha_\nu+1)E/\langle E_\nu \rangle}, \quad (20)$$

where the parameter  $\alpha_\nu$  is defined by  $\langle E_\nu^2 \rangle / \langle E_\nu \rangle^2 = (2 + \alpha_\nu) / (1 + \alpha_\nu)$  and  $\xi_\nu$  is a normalization factor such that  $\int f_\nu(E) dE = 1$ .

In order to incorporate neutrino oscillations in our nucleosynthesis computations, we consider the 7 selected post-bounce times  $t_0$  as representative of the changing wind conditions during the proto-neutron star cooling phase (note the partial overlap with data from the simulation by Hüpdepohl et al. 2010 used for the analysis in Tamborra et al. 2012b). In Table 1 we list the neutrinosphere radius  $R_\nu$  (assumed to be equal for all flavors), the luminosity  $L_\nu$ , the mean energy  $\langle E_\nu \rangle$ , and the fit exponent  $\alpha_\nu$  for each neutrino flavor and for the seven representative wind trajectories.

In what follows, we neglect oscillations driven by the smallest mass difference between the active flavors,  $\delta m_{\text{sol}}$ , and focus on neutrino oscillations in the active sector driven by the largest mass difference between  $\nu_e$  and  $\nu_x$ ,  $\delta m_{\text{atm}}$ , and by the mixing angle  $\theta_{13}$ . The reduction to two effective active flavors is justified since oscillations driven by the solar parameters tend to take place at a larger radius than the ones driven by  $\delta m_{\text{atm}}$  and are, therefore, unlikely to affect SN nucleosynthesis (see Dasgupta & Dighe 2008; Fogli et al. 2009a; Dasgupta et al. 2010 for details). Concerning active-sterile oscillations, we consider the mixing of only the electron neutrino flavor with a light sterile state for simplicity. Overall, we discuss a 2-flavor scenario (2 active flavors,  $\nu_e$  and  $\nu_x$ ) as well as a 3-flavor one (2 active+1 sterile flavors,  $\nu_e$ ,  $\nu_x$  and  $\nu_s$ ).

If interpreted in terms of sterile neutrinos  $\nu_s$ , the reactor antineutrino anomaly requires a mass difference in the eV range, and cosmological hot dark matter limits imply that the sterile state would have to be heavier than the active flavors (Abazajian et al. 2012). We here adopt the following mass splittings (Capozzi et al. 2013; Mention et al. 2011):

$$\delta m_{\text{atm}}^2 = -2.35 \times 10^{-3} \text{ eV}^2 \quad \text{and} \quad \delta m_s^2 = 2.35 \text{ eV}^2, \quad (21)$$

with  $\delta m_{\text{atm}}^2$  being the squared mass difference between the neutrino mass eigenstates  $\nu_3$  and the remaining two  $\nu_{1,2}$  (Fogli et al. 2006) and  $\delta m_s^2$  the squared mass difference between the neutrino mass eigenstate  $\nu_4$  and  $\nu_1$ , chosen to be representative of reactor-inspired values. We assume normal hierarchy for the sterile mass-squared difference, namely  $\delta m_s^2 > 0$  (i.e. the neutrino mass eigenstate  $\nu_4$  is heavier than the other mass eigenstates associated to the active neutrino flavors) and inverted mass hierarchy for the atmospheric difference,  $\delta m_{\text{atm}}^2 < 0$  (meaning that the neutrino mass eigenstate  $\nu_3$  is lighter than  $\nu_{1,2}$  Fogli et al. 2006). Note that current global fits of short-baseline neutrino experiments estimate  $0.82 \leq \delta m_s^2 \leq 2.19 \text{ eV}^2$  at  $3\sigma$  of confidence level (Giunti et al. 2013), which is lower than our adopted reference value (Mention et al. 2011). Our conservative choice favors a comparison with previous results discussed in Tamborra et al. (2012b) besides not qualitatively changing

our conclusions. We choose to scan only the inverted hierarchy scenario in the active sector (i.e.,  $\delta m_{\text{atm}}^2 < 0$ ), since this is the case where the largest impact due to collective flavor oscillations on nucleosynthesis is expected (Hannestad et al. 2006; Fogli et al. 2007, 2008; Dasgupta et al. 2010). The associated ‘‘high’’ (H) and ‘‘sterile’’ (S) vacuum oscillation frequencies are then:

$$\omega_{\text{H}} = \frac{\delta m_{\text{atm}}^2}{2E} \quad \text{and} \quad \omega_{\text{S}} = \frac{\delta m_s^2}{2E}, \quad (22)$$

with  $E$  being the neutrino energy. For the mixing angles we use (Capozzi et al. 2013; Mention et al. 2011):

$$\sin^2 2\theta_{14} = 10^{-1} \quad \text{and} \quad \sin^2 \theta_{13} = 2 \times 10^{-2}. \quad (23)$$

We treat neutrino oscillations in terms of matrices of neutrino densities  $\rho_E$  for each energy mode  $E$ . The diagonal elements of the density matrices are related to the neutrino densities, while the off-diagonal ones encode phase information. The radial flavor evolution of the neutrino flux is given by the ‘‘Schrödinger equations,’’

$$i\partial_r \rho_E = [\mathbf{H}_E, \rho_E] \quad \text{and} \quad i\partial_r \bar{\rho}_E = [\bar{\mathbf{H}}_E, \bar{\rho}_E], \quad (24)$$

where an overbar refers to antineutrinos and sans-serif letters denote  $3 \times 3$  matrices in the  $\nu_e, \nu_x, \nu_s$  flavor space. The initial conditions for the density matrices are  $\rho_E = \text{diag}(n_{\nu_e}, n_{\nu_x}, 0)$  and  $\bar{\rho}_E = \text{diag}(n_{\bar{\nu}_e}, n_{\bar{\nu}_x}, 0)$ , i.e., we assume that sterile neutrinos are generated by flavor oscillations. The Hamiltonian matrix consists of the vacuum, matter and neutrino self-interaction terms:

$$\mathbf{H}_E = \mathbf{H}_E^{\text{vac}} + \mathbf{H}_E^{\text{m}} + \mathbf{H}_E^{\nu\nu}. \quad (25)$$

In the flavor basis, the vacuum term,

$$\mathbf{H}_E^{\text{vac}} = \mathbf{U} \text{diag} \left( -\frac{\omega_{\text{H}}}{2}, +\frac{\omega_{\text{H}}}{2}, \omega_{\text{S}} \right) \mathbf{U}^\dagger, \quad (26)$$

is a function of the mass-squared differences (see Eq. 22) (with  $\mathbf{U}$  being the unitary matrix transforming between the mass and the interaction basis) and of the mixing angles. The matter term in the flavor basis spanned by  $(\nu_e, \nu_x, \nu_s)$  is:

$$\mathbf{H}_E^{\text{m}} = \sqrt{2} G_{\text{F}} \text{diag} \left( N_e - \frac{N_n}{2}, -\frac{N_n}{2}, 0 \right), \quad (27)$$

where  $N_e$  is the net electron number density and  $N_n$  the neutron density. Using Eq. (1), the matter term becomes:

$$\mathbf{H}_E^{\text{m}} = \sqrt{2} G_{\text{F}} N_b \text{diag} \left( \frac{3}{2} Y_e - \frac{1}{2}, \frac{1}{2} Y_e - \frac{1}{2}, 0 \right), \quad (28)$$

with  $N_b$  being the baryon density. Note that the matter potential can be positive or negative and for  $Y_e > 1/3$  ( $Y_e < 1/3$ ) a  $\nu_e$ - $\nu_s$  ( $\bar{\nu}_e$ - $\bar{\nu}_s$ ) MSW resonance can occur (Mikheyev & Smirnov 1985; Nunokawa et al. 1997; McLaughlin et al. 1999; Fetter 2000). Because of Eq. (28) neutrinos feel a different matter potential as  $Y_e$  changes and, at the same time,  $Y_e$  is affected by neutrino oscillations via Eq. (4).

The  $\mathbf{H}_E^{\nu\nu}$  term describes  $\nu$ - $\nu$  interactions and vanishes for all elements involving sterile neutrinos (Sigl & Raffelt 1993), i.e.  $\mathbf{H}_{es}^{\nu\nu} = \mathbf{H}_{xs}^{\nu\nu} = \mathbf{H}_{ss}^{\nu\nu} = 0$  (i.e., the only non-vanishing off-diagonal element of the  $3 \times 3$  matrix is  $\mathbf{H}_{ex}^{\nu\nu}$ , see Tamborra et al. 2012b for further details). In the treatment of  $\nu$ - $\nu$  interactions, for the sake of simplicity, we assume the so-called single-angle approximation, i.e. all neutrinos feel the same

<sup>10</sup> In Eq. (19), general relativistic redshift corrections, which depend on  $r$ , as well as a ‘‘flux factor’’ accounting for nonradial neutrino momenta close to the neutrinosphere, are ignored.

average neutrino-neutrino refractive effect (Duan et al. 2006; Fogli et al. 2007; Duan et al. 2010). It will become clear in the following, that such an assumption does not compromise our conclusions.

In what follows, we explore the impact of active-active and active-sterile neutrino conversions on the nucleosynthesis conditions and nucleosynthetic yields for the 7 representative trajectories corresponding to postbounce times  $t_0$ . We distinguish two scenarios:

1. “Active” case: Neutrino oscillations in the active sector (2 active states).
2. “Sterile” case: Neutrino oscillations in the active and sterile sectors (2 active states + 1 sterile state).

#### 5. INFLUENCE OF NEUTRINO OSCILLATIONS AND $\alpha$ -EFFECT ON THE ELECTRON FRACTION

In this section, we discuss the evolution of  $Y_e$  as a function of radius for our selected postbounce times ( $t_0 = 0.5, 1, 2, 2.9, 4.5, 6.5,$  and  $7.5$  s), for the scenarios 1 and 2 introduced in Sect. 4, and with the two  $X_\alpha$  cases (i) and (ii) (see Sect. 3). As discussed in Tamborra et al. (2012b), conversions of active neutrinos to sterile states as well as collective oscillations between the active flavors influence the asymptotic value of  $Y_e$  in the neutrino-driven wind in time-dependent and complicated ways.

While neutrinos propagate out from the SN core, the MSW resonance conditions between active flavors and light sterile neutrinos are verified in two different spatial regions and might affect the ejecta  $Y_e$  and the nucleosynthesis outcome (see extended discussion in Nunokawa et al. 1997). Close to the neutrinosphere, due to the steep growth of  $Y_e$ , and therefore of the matter potential (Eq. 28), active-sterile MSW resonances are verified for both neutrinos and antineutrinos within a very small spatial region. At larger radii (which move closer to the neutrinosphere as the postbounce time increases), a second outer MSW resonance occurs and is mainly relevant for neutrinos, although it might even affect antineutrinos because of the feedback effects on  $Y_e$  due to oscillations (see Tamborra et al. 2012b for more details).

The outer MSW resonance is generally adiabatic: It occurs where the matter potential is shallow and the effective mixing angle is larger. Therefore  $\nu_e$  are abundantly converted in  $\nu_s$ , lowering the wind  $Y_e$  (see Eqs. 4, 5, 6) because of the feedback effect as we will discuss later. On the other hand, the inner MSW resonance is mostly non-adiabatic: It occurs where the matter potential is very steep and the effective mixing angle small. As a consequence, conversions of  $\nu_e$  and  $\bar{\nu}_e$  to sterile states are mostly inhibited except for the very low-energy tails of the energy spectra, practically having a negligible role on  $Y_e$  during the cooling phase (Nunokawa et al. 1997, Wu et al. 2014). As pointed out in Wu et al. (2014), the inner resonance may instead be responsible for non-negligible effects during the accretion phase where a wider energy range of  $\nu_e$  ( $\bar{\nu}_e$ ) may be converted to sterile states, because the growth of  $Y_e$  close to the neutrinosphere is less steep.

In what follows, due to the numerical complexity of the feedback effect in the presence of neutrino self-interactions within our (2+1) neutrino-family scenario, we will neglect the inner resonance in the numerical computations where not otherwise specified, whereas we include the outer one as well as collective oscillations (since both of them are expected to have a larger impact on  $Y_e$ ). Note that in the region where

the inner resonance occurs, also collective oscillations are not expected to play any role. The robustness of our approximation is supported by numerical tests, where within a simplified numerical setup (i.e. without neutrino self-interactions), we have tested the negligible impact of the inner resonance on  $Y_e$  for the earlier postbounce times of the studied neutrino cooling phase of our ECSN.

The outer  $\nu_e$ - $\nu_s$  MSW conversion depletes the  $\nu_e$  flux, favoring a neutron-rich site. Therefore, in general, the main effect of oscillations expected in the presence of sterile neutrinos is a reduction of  $Y_e$  relative to the case without oscillations. This effect is particularly evident in the early explosion phase where the outer  $\nu_e$ - $\nu_s$  MSW resonance driven by  $\Delta m_s^2$  is dominated by the Hamiltonian of ordinary matter and leads to a complete  $\nu_e$ - $\nu_s$  swap with little or no trace of  $\nu$ - $\nu$  collective oscillations (cf. for example  $t_0 = 0.5$  s in Tamborra et al. 2012b and Wu et al. 2014 for details). Still, the effect on the ejecta  $Y_e$  was moderate because the MSW conversion took place at large radii where  $Y_e$  had nearly reached its terminal value. At later times (see  $t_0 = 6.5$  s in Tamborra et al. 2012b), the  $\nu$ - $\nu$  refraction strongly reduces the matter effect, largely compensating the overall  $\nu_e$ - $\nu_s$  MSW conversion. The resultant effect of  $\nu$ - $\nu$  interactions is that they repopulate the  $\nu_e$  flux (because of  $\nu_x$ - $\nu_e$  conversions) and partially counterbalance the effect of  $\nu_e$ - $\nu_s$  MSW resonances on the electron abundance (Tamborra et al. 2012b). Note that, for simplicity, in our computations we consider the effects of energy-dependent features of the oscillated neutrino spectra on  $Y_e$  evolution (Tamborra et al. 2012b) in an integral sense by adopting neutrino spectral quantities averaged over energy in Eqs. (7, 8).

The evolution of the electron fraction is not just influenced by the  $\nu_e$  and  $\bar{\nu}_e$  properties, which are affected by the neutrino oscillations, but also by the presence of the  $\alpha$  particles, see Eqs. (4), (15) and (16). Therefore, the whole  $Y_e$  evolution is a complicated interplay between neutrino oscillations and the  $\alpha$ -effect associated with the formation of  $\alpha$  particles, and the outcome depends on the relative location of the regions of active-sterile conversion and  $\alpha$ -particle formation. For this reason, we choose to analyze the  $Y_e$  evolution in detail for two representative postbounce times,  $t_0 = 2.9$  s and  $t_0 = 6.5$  s.

In order to clarify the expected effects on  $Y_e$ , we show in Fig. 3 (left panel) the luminosities and mean energies for  $\nu_e$  and  $\bar{\nu}_e$  as functions of radius for the “active” and “sterile” cases for  $t_0 = 2.9$  s. In the active case, neutrino oscillations do not visibly modify the mean energies and the luminosities in the radial regime where  $Y_e$  is still evolving (i.e.  $r \lesssim 2 \times 10^7$  cm). This is due to the fact that for our initial conditions for neutrinos and antineutrinos (i.e.,  $L_{\nu_e, \bar{\nu}_e} / \langle E_{\nu_e, \bar{\nu}_e} \rangle - L_{\nu_x} / \langle E_{\nu_x} \rangle < 0$ ), multiple spectral splits should be expected for an inverted hierarchy (Fogli et al. 2009b). However, since the  $\nu_e$  and  $\bar{\nu}_e$  luminosities and mean energies are very similar to those of heavy-lepton neutrinos, as shown in Table 1, and because of the total lepton-number conservation, no appreciable variations occur in the oscillated luminosities and mean energies (see Fogli et al. 2009b for an extended discussion on the topic). As a consequence, we do not expect any appreciable effect on  $Y_e$ . In contrast, in the sterile case an important effect of neutrino oscillations happens at  $r \simeq 0.5 \times 10^7$  cm (Fig. 3, left panel), where  $\nu_s$  are copiously produced through an MSW resonance at the expense of only  $\nu_e$  (for more details, see also the results for  $t_0 = 2.9$  s in Tamborra et al. 2012b).

This means that the  $\nu_e$  number flux (defined by  $L_{\nu_e} / \langle E_{\nu_e} \rangle$ ) in the “sterile” case is much lower than in the “active” one for

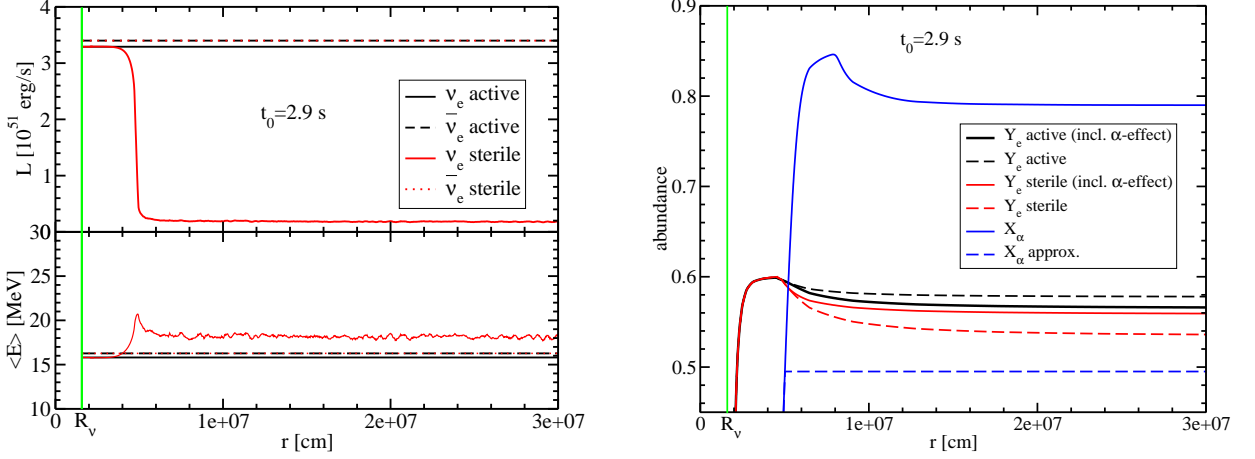


FIG. 3.— *Left*: Electron neutrino and antineutrino luminosities ( $L_{\nu_e}$  and  $L_{\bar{\nu}_e}$ ) in units of  $10^{51}$  erg/s (upper panel) and mean energies ( $\langle E_{\nu_e} \rangle$  and  $\langle E_{\bar{\nu}_e} \rangle$ ; lower panel) as functions of the distance ( $r$ ) from the center of the PNS at  $t_0 = 2.9$  s postbounce. (The solid red lines are computed as running averages over  $\Delta r \approx 1.98 \cdot 10^5$  cm.) In the “active” case the luminosities and mean energies for both  $\nu_e$  and  $\bar{\nu}_e$  are constant outside of the neutrinosphere  $R_\nu$ , which implies that the “active” case does not show any significant variations from the case without  $\nu$  oscillations for the studied ECSN progenitor. In the “sterile” case a  $\nu_e$ - $\nu_s$  MSW resonance occurs at  $r \approx 0.50 \times 10^7$  cm. *Right*: Electron fraction  $Y_e$  and  $\alpha$  mass fraction  $X_\alpha$  as functions of distance  $r$  from the center of the PNS at  $t_0 = 2.9$  s. In the active scenario (see case 1, Sect. 4) neutrino oscillations negligibly affect  $Y_e$  (same as the no oscillations case; not shown here). In the sterile scenario (case 2, Sect. 4), neutrino oscillations affect  $Y_e$  when  $\alpha$  particles start forming. The solid lines (“incl.  $\alpha$ -effect” cases) refer to  $Y_e$  obtained when full network calculations were performed (the corresponding  $X_\alpha$  is also shown with the solid blue line), while the dashed  $Y_e$  lines refer to calculations corresponding to case (ii) in Sect. 3 (the corresponding  $X_\alpha$  is also shown by a dashed blue line).

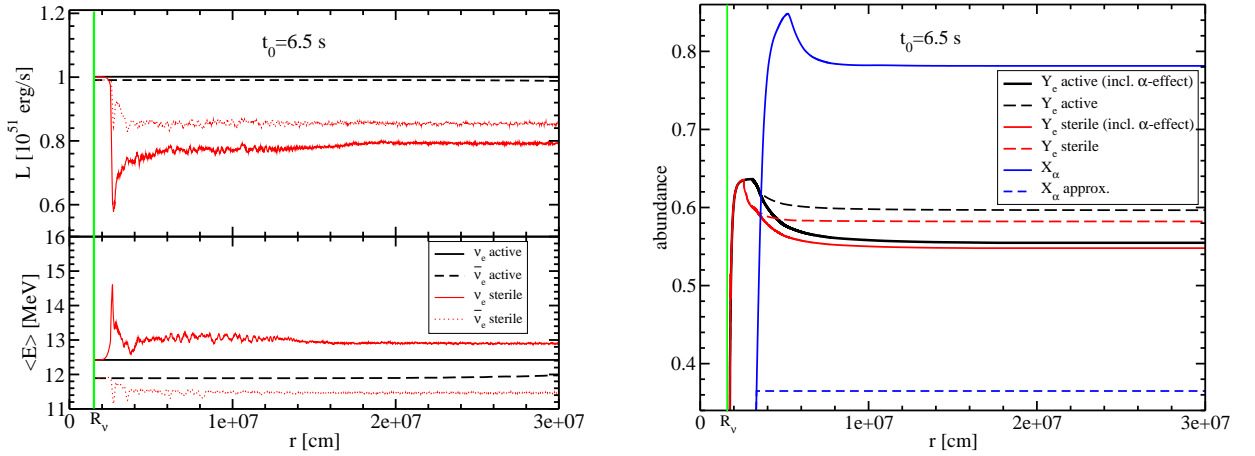


FIG. 4.— *Left*: Electron neutrino and antineutrino luminosities ( $L_{\nu_e}$  and  $L_{\bar{\nu}_e}$ ; upper panel) in units of  $10^{51}$  erg/s for  $t_0 = 6.5$  s as functions of the distance ( $r$ ) from the center of the PNS for “active” and “sterile” cases. Lower panel: Similar to the upper panel, but for the mean energies ( $\langle E_{\nu_e} \rangle$  and  $\langle E_{\bar{\nu}_e} \rangle$ ). (The red lines display running averages over  $\Delta r \approx 1.1 \cdot 10^5$  cm.) In the sterile case a  $\nu_e$ - $\nu_s$  MSW resonance occurs at  $r \approx 0.3 \times 10^7$  cm, triggering collective oscillations at larger radii. *Right*: Electron fraction  $Y_e$  and  $\alpha$  mass fraction  $X_\alpha$  as functions of distance  $r$  from the center of the PNS at  $t_0 = 6.5$  s. In the “active” scenario (see case 1, Sect. 4) neutrino oscillations negligibly affect  $Y_e$  (same as the no oscillations case; not shown), while in the “sterile” scenario (case 2, Sect. 4), neutrino oscillations affect  $Y_e$  very close to the neutrinosphere  $R_\nu$ . The solid lines refer to  $Y_e$  obtained when full network calculations were used (the corresponding  $X_\alpha$  is also shown), while the dashed  $Y_e$  lines refer to the case of incomplete nucleon recombination to  $\alpha$  particles (see case (ii) in Sect. 3).

$r > 0.50 \times 10^7$  cm, while the  $\bar{\nu}_e$  flux remains unchanged.

To demonstrate the effect of the modified neutrino properties on  $Y_e$  via Eq. (4), we plot  $Y_e$  as a function of the radius for  $t_0 = 2.9$  s in Fig. 3 (right panel). Since in the “active” case, oscillations do not appreciably affect the neutrino luminosities and mean energies up to the radius of interest, the  $Y_e$  evolution does not differ from the case without neutrino oscillations.

At  $r > 0.50 \times 10^7$  cm the results of simulations with and without  $\alpha$ -particle formation from free nucleons can be discriminated because of the  $\alpha$ -effect, associated with the presence of large abundances of  $\alpha$  particles, which has severe consequences for the  $Y_e$  evolution. The abundances of  $\alpha$  particles for our two cases (i) and (ii) are displayed by solid (“incl.  $\alpha$ -effect”) and dashed blue lines, respectively, and the corresponding  $Y_e$  histories by solid and dashed black and

red lines. First let us consider the case in which the  $\alpha$ -particle abundance is frozen at a low level, case (ii), following Tamborra et al. (2012b) (i.e., dashed lines in Fig. 3, right panel): The MSW conversion of  $\nu_e$  to sterile neutrinos  $\nu_s$  (visible by the steep drop of  $L_{\nu_e}$  at  $r \approx 0.5 \times 10^7$  cm in Fig. 3 and reflected by the kink of the  $Y_e$  curves at this radius) causes a reduction of  $Y_e$  in the sterile case (red dashed line) compared to the active case (black dashed line). This decrease can be easily understood by the suppression of  $\nu_e$  absorptions on free neutrons (see Eq. 4). However, despite the dramatic drop of  $L_{\nu_e}$  the effect on  $Y_e$  is relatively modest (insufficient to drive  $Y_e$  to the neutron-rich side) because neutrino reactions with nucleons are diminished by the wind expanding in its outward acceleration away from the neutrinosphere. The  $Y_e$  reduction (reaching  $Y_e \sim 0.54$  for  $r \rightarrow \infty$ ), is even less strong than

found by Tamborra et al. (2012b), who obtained  $Y_e \simeq 0.46$  for  $t_0 = 2.9$  s, because weak magnetism and recoil corrections in Eqs. (7) and (8) were neglected in that previous work. According to Horowitz & Li (1999) the weak magnetism and recoil corrections lead to a slight increase of the charged-current absorption cross section of  $\nu_e$  on neutrons and a larger reduction of  $\bar{\nu}_e$  absorption on protons (cf. Eqs. 7, 8) and therefore damp the tendency towards lower  $Y_e$ . In contrast, the results with  $\alpha$ -effect (case (i); solid red and black lines in Fig. 3, right panel) show a counterintuitive behavior. The cases with active flavor oscillations (black solid line) and sterile flavor oscillations (red solid line) approach nearly the same asymptotic value of  $Y_e$ . While for active flavor oscillations the  $\alpha$ -effect drives  $Y_e$  closer to 0.5 in the usual way (compare the black dashed and solid lines in Fig. 3, right panel), the sterile neutrino case exhibits the opposite behavior: In the presence of a higher abundance of  $\alpha$ -particles, i.e. despite the  $\alpha$ -effect,  $Y_e$  remains higher and the evolution towards  $Y_e \simeq 0.5$  is clearly damped (red solid line in comparison to red dashed line). The formation of a larger abundance of  $\alpha$ -particles thus obviously reduces the influence of the active-sterile conversions. This astonishing result is a consequence of the fact that the conversion to sterile neutrinos occurs slightly outside (or overlaps with) the region where the rapid recombination of neutrons and protons to  $\alpha$ -particles takes place. In such a situation the influence of the  $\nu_e$ - $\nu_s$  conversions on the  $Y_e$  evolution is diminished by the lower number fractions of free neutrons and protons, which lead to a lower rate of change of  $Y_e$  according to Eq. (4). Instead of undergoing reactions with  $\nu_e$  or  $\bar{\nu}_e$ , the majority of free nucleons is absorbed in  $\alpha$ -particles as the wind expands away from the  $\nu_e$ - $\nu_s$  conversion radius. The proximity of the asymptotic  $Y_e$  values for the active and sterile cases including  $\alpha$ -effect is somewhat incidental (i.e. a consequence of especially “fine-tuned” conditions) as can be seen by a second exemplary case discussed in the following.

The influence of  $\alpha$ -particle formation manifests itself differently in the late wind evolution, where  $\nu_e$  conversion to sterile neutrinos takes place closer to the neutrinosphere and therefore below the radius at which nucleon recombination begins to raise the  $\alpha$  abundance.

In order to explain the interplay between neutrino oscillations and  $\alpha$ -effect in the  $Y_e$  evolution for the late phases of the proto-neutron star cooling, we show in Fig. 4 luminosities and mean energies for  $\nu_e$  and  $\bar{\nu}_e$  at the postbounce time  $t_0 = 6.5$  s (in analogy to Fig. 3). Analog to the case of  $t_0 = 2.9$  s, due to the similar neutrino fluxes and spectra, neutrino oscillations do not change the values of the luminosities and mean energies in the active case. In the sterile case instead, the neutrino oscillations occur very close to the neutrinosphere. In this case, an MSW resonance occurs already at about  $r \simeq 0.25 \times 10^7$  cm for  $\nu$  and  $\bar{\nu}$  (see Tamborra et al. 2012b for more details). The MSW resonance reduces the  $\nu_e$  number flux (i.e.  $L_{\nu_e}/\langle E_{\nu_e} \rangle$ ) significantly compared to the  $\bar{\nu}_e$  number flux. This means that the neutrino oscillations favor a more neutron-rich environment (i.e., a lower  $Y_e$ ) compared to the active case (see reactions (2,3), and Eq. (4)).

Figure 4 (right panel) shows the evolution of the electron fraction  $Y_e$  for  $t_0 = 6.5$  s, for the active and sterile cases, in analogy to Fig. 3 (right panel). The dashed lines are again calculated without the  $\alpha$ -effect.  $Y_e$  in the sterile case (red dashed line) is lower than in the active case (black dashed line) already very close to the neutrinosphere where the matter is still disintegrated in free nucleons in NSE and thus no  $\alpha$  particles are present.

When the  $\alpha$ -effect is included, the value of  $Y_e$  is, as expected, pushed towards 0.5 in both active (black solid line) and sterile cases (red solid line). We notice that for  $t_0 = 6.5$  s, different from  $t_0 = 2.9$  s, the neutrino flavor conversions take place *before* the  $\alpha$  particles start forming and therefore they make the environment less proton-rich ( $Y_e$  is lowered) before the  $\alpha$ -effect takes place and decreases  $Y_e$  even further towards more symmetric conditions ( $Y_e = 0.5$ ).

Figure 5 presents an overview of the interplay between neutrino oscillations and the  $\alpha$ -effect by showing the evolution of the electron fraction  $Y_e$  for all considered postbounce times  $t_0$ . Figure 5 (left panel) shows  $Y_e$  as functions of the distance  $r$  from the center of the PNS at different postbounce times  $t_0$  for both the “active” and “sterile” cases including the  $\alpha$ -effect. For the early postbounce times ( $t_0 = 0.5, 1, 2$  s),  $Y_e$  in the “sterile” case is about the same as in the “active” case, making the role of sterile neutrinos almost negligible. For the intermediate and late postbounce times ( $t_0 = 2.9, 4.5, 6.5, 7.5$  s),  $Y_e$  is always lower in the “sterile” case compared to the “active” case.

In Fig. 5 (right panel) the asymptotic  $Y_e$  values (namely,  $Y_e$  at  $r \simeq 3 \cdot 10^7$  cm) are plotted as functions of the postbounce time for each of the considered scenarios (“active”, “sterile” and no oscillations cases). Note that the values for the “active” case cannot be distinguished from those for the case without oscillations, essentially suggesting negligible roles of the active-active oscillations on the evolution of  $Y_e$  for the discussed SN model. Comparing the dashed lines for the “active” and “sterile” cases confirms that  $Y_e$  in the “sterile” case is systematically lower than in the “active” case because of the  $\nu_e$ - $\nu_s$  conversions. However, since the whole picture is the result of a complex interplay between non-linear collective flavor oscillations and MSW resonances for the sterile state (see Tamborra et al. 2012b), the efficiency of sterile neutrinos in lowering  $Y_e$  is strongly time dependent.

Comparing the black dashed curve with the solid one (the latter including the  $\alpha$ -effect),  $Y_e$  is systematically pushed towards 0.5 by the  $\alpha$ -effect in the “active” case. In the “sterile” case, neutrino oscillations combined with the  $\alpha$ -effect lead to  $Y_e$  being almost the same as in the “active” case at early and intermediate postbounce times (compare the red solid line with the black solid line).

At late times and including the  $\alpha$ -effect,  $Y_e$  in the “sterile” case becomes lower than  $Y_e$  in the “active” case and lower than  $Y_e$  in the case without full  $\alpha$  recombination because the MSW  $\nu_e$ - $\nu_s$  conversion happens so close to the neutrinosphere that the  $\alpha$  particle formation at larger radii further enhances the  $Y_e$ -reduction associated with the presence of sterile neutrinos.

We remark that in the paper of Wu et al. (2014) active-sterile MSW oscillations in the very early neutrino-driven ejecta (which are not object of the study of this work) lower  $Y_e$  considerably, in contrast to our findings at the earlier postbounce times  $t_0$ , and even more strongly than we observe at late postbounce times. The reasons for these differences are twofold. On the one hand,  $\alpha$  particles in the early, very hot ejecta form only at large radii, making the  $\alpha$ -effect unimportant for the  $Y_e$  setting. On the other hand, the assumed multi-angle matter effect suppresses self-induced neutrino-flavor conversions in the dense material of the early ejecta (Sarikas et al. 2012; Raffelt et al. 2013; Chakraborty et al. 2011). Therefore, in the phase considered by Wu et al. (2014),  $\nu_e$ - $\nu_s$  MSW transitions are the main effect, leading to a reduced ejecta  $Y_e$ . This means that neither

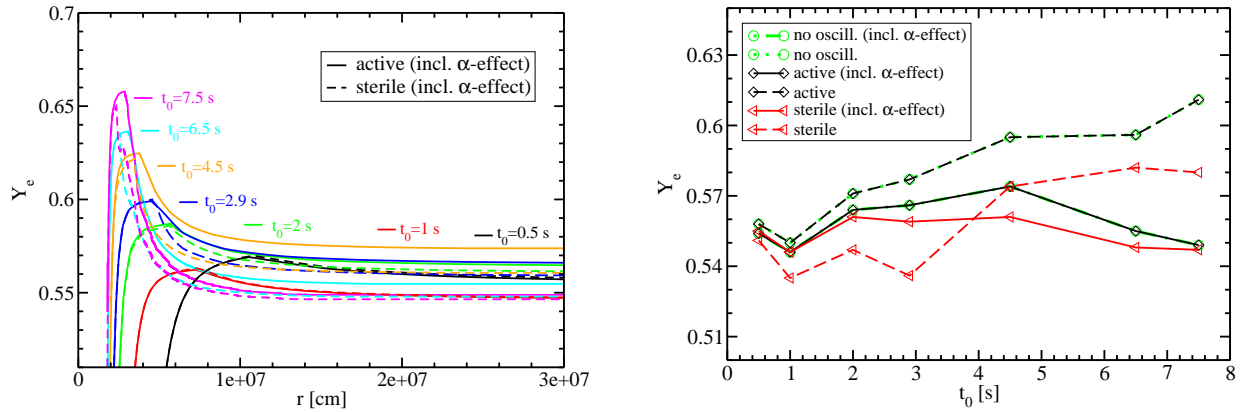


FIG. 5.— *Left*: Electron fraction ( $Y_e$ ) as a function of the distance  $r$  from the center of the PNS for all considered postbounce times ( $t_0$ ), and for “active” and “sterile” cases. The  $\alpha$ -effect is included in all cases (“incl.  $\alpha$ -effect”). Because of the near equality of the neutrino luminosities and mean energies of neutrinos of all flavors,  $Y_e$  in the “active” cases does not appreciably differ from the one obtained without neutrino oscillations. *Right*: Asymptotic electron fractions ( $Y_e$ ) as functions of postbounce time ( $t_0$ ) for “active” and “sterile” as well as no oscillations cases. The dashed lines refer to  $Y_e$  calculated without the  $\alpha$ -effect, while the solid lines refer to  $Y_e$  calculated with the full network. The  $\alpha$ -effect is stronger especially at late times ( $t_0 = 6.5$  and  $7.5$  s) when the neutron star is more compact and the neutrino luminosities are lower. The values for the cases without oscillations coincide with those for the “active” cases and cannot be distinguished.

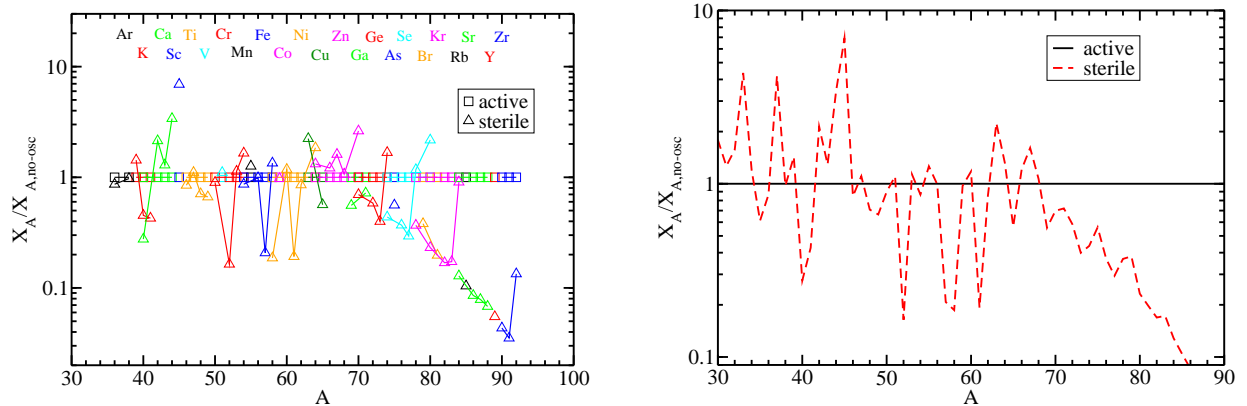


FIG. 6.— *Left*: Isotopic mass fractions for the “active” and “sterile” cases relative to those for the case without oscillations versus mass number  $A$  for all representative 7 trajectories. *Right*: Nucleosynthetic abundances for the “active” and “sterile” cases relative to those without oscillations for all the representative 7 trajectories. Since in our model active flavor oscillations do not change the neutrino properties and the wind  $Y_e$  at any significant level up to the radius of interest, the nucleosynthesis results are essentially identical for all the cases with active oscillations and no neutrino oscillations.

the  $\alpha$ -effect nor the  $\nu$ - $\nu$  interactions play the crucial roles that we attribute to them in the interpretation of the  $Y_e$  evolution for the later  $\nu$ -driven wind.

The  $\alpha$ -effect plays an important role in lowering  $Y_e$  in particular at late times ( $t_0 = 4.5, 6.5$  and  $7.5$  s). This is a consequence of the higher wind entropy and the longer expansion timescale as a result of the more compact PNS with lower neutrino luminosities, resulting in a delay of the  $\alpha$  recombination relative to the  $\nu_e$ - $\nu_s$  conversion and in a longer duration of the  $\alpha$ -effect (see also next section for more details). However, although the  $\alpha$ -effect has a strong impact on  $Y_e$  and therefore on the element production, it plays a sub-leading role for the neutrino oscillations since it does not drastically modify the matter potential felt by neutrinos; therefore, no detectable modifications are expected for the neutrino fluxes at the Earth.

Because of the crucial role of the  $\alpha$ -effect on  $Y_e$  in the context of flavor oscillations, especially at early and late times, where  $Y_e$  for “active” and “sterile” cases including  $\alpha$ -effect is fairly similar (see Fig. 5, right panel), we expect that the nucleosynthesis yields in the presence of neutrino oscillations are not significantly different from the cases where oscillations are not considered (see Sect. 3.1). This can be seen in Fig. 6, where we show the nucleosynthesis yields obtained for the 7 representative trajectories in the “active” and “ster-

ile” cases relative to those without neutrino oscillations. In Fig. 6 (left panel) we notice that most of the isotopic mass fraction ratios in the “sterile” case relative to the “no oscillation” case are between roughly 0.5 and 2. The most abundantly produced isotope in the relative comparison is  $^{45}\text{Sc}$  ( $X_{\text{sterile}}^{45\text{Sc}}/X_{\text{no-osc.}}^{45\text{Sc}} \approx 7$ ). This overproduction of the  $^{45}\text{Sc}$  isotope in the “sterile” case compared to the case without oscillations, however, is too small to have any significant impact on the production factor of this isotope (see Fig. 2, right panel). From Fig. 6, it is also clear that in the “sterile” case, there is less production of heavy elements (e.g.  $A \geq 80$ ) than in the case without oscillations.

From Figs. 5 and 6, one can conclude that neither active neutrino oscillations nor a fourth sterile neutrino family can alter the nucleosynthesis-relevant conditions fundamentally, nor can they create a neutron-rich site ( $Y_e < 0.5$ ) to activate the r-process in the adopted ECSN model (without nucleon potential corrections in the high-density neutrino opacities; see Section 6).

## 6. NEUTRINO OSCILLATIONS IN A NEUTRON-RICH WIND

In the previous sections, we considered neutrino oscillation effects in the proton-rich environment obtained in the models of Hüpdepohl et al. (2010). As mentioned in Sect. 1,

TABLE 2  
TOY MODEL PARAMETERS EMULATING MEAN-FIELD NUCLEON POTENTIAL CORRECTIONS ON THE NEUTRINO OPACITIES<sup>a</sup>.

$t_0^b$ [s]	$L_{\nu_e}^c$ [ $10^{51}$ erg/s]	$L_{\bar{\nu}_e}^d$ [ $10^{51}$ erg/s]	$L_{\nu_e}/\langle E_{\nu_e} \rangle^e$ [ $10^{56}$ s <sup>-1</sup> ]	$L_{\bar{\nu}_e}/\langle E_{\bar{\nu}_e} \rangle^f$ [ $10^{56}$ s <sup>-1</sup> ]	$\langle E_{\nu_e} \rangle^g$ [MeV]	$\langle E_{\bar{\nu}_e} \rangle^h$ [MeV]	$Y_{e,a}^i$	$Y_{e,a}^{X_\alpha=0}^j$	$Y_{e,a}^{\text{act}}^k$	$Y_{e,a}^{\text{ste}}^l$
2.9	<b>3.30</b>	<b>3.40</b>	3.268	1.099	6.3	19.3	0.422	0.403	0.422	0.430
6.5	<b>1.00</b>	<b>0.99</b>	1.248	0.325	5.0	19.0	0.428	0.368	0.428	0.510
2.9	1.670	2.899	<b>1.303</b>	<b>1.302</b>	8.0	13.9	0.420	0.405	0.421	0.440
6.5	0.645	1.165	<b>0.499</b>	<b>0.518</b>	8.0	14.0	0.431	0.380	0.431	0.486

<sup>a</sup> In the first two cases we keep the neutrinospheric neutrino luminosities as given by the hydrodynamic simulations (Table 1), while in the last two cases we keep the neutrinospheric neutrino number fluxes as given by the hydrodynamic simulations, in both cases marked by boldfacing.

<sup>b</sup> Postbounce time.

<sup>c,d</sup> Neutrinospheric luminosities of  $\nu_e$  and  $\bar{\nu}_e$ , respectively.

<sup>e,f</sup> Neutrinospheric number fluxes of  $\nu_e$  and  $\bar{\nu}_e$ , respectively.

<sup>g,h</sup> Neutrinospheric mean energies of  $\nu_e$  and  $\bar{\nu}_e$ , respectively.

<sup>i</sup> Asymptotic wind electron fraction taking into account the  $\alpha$ -effect.

<sup>j</sup> Asymptotic wind electron fraction without taking into account the  $\alpha$ -effect ( $X_\alpha = 0$ ).

<sup>k</sup> Asymptotic wind electron fraction taking into account neutrino oscillations in the active sector and  $\alpha$ -effect.

<sup>l</sup> Asymptotic wind electron fraction taking into account neutrino oscillations in the active and sterile sectors as well as  $\alpha$ -effect.

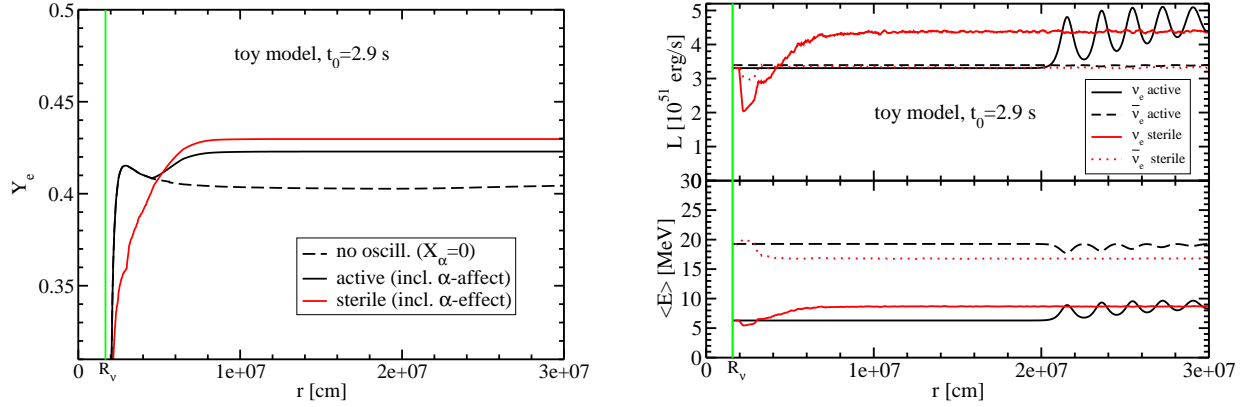


FIG. 7.— *Left*: Electron fraction  $Y_e$  as function of distance  $r$  from the center of the PNS for our toy model at  $t_0 = 2.9$  s (see text for details) for the case without neutrino oscillations and setting  $X_\alpha = 0$  (“no oscill. ( $X_\alpha = 0$ )” case, dashed black line), for the case with flavor conversions of active neutrinos (solid black line), and for the case of active-sterile conversions (solid red line). Both of the last two cases were computed with  $\alpha$  particle recombination. Neutrino oscillations, jointly with the  $\alpha$ -effect, drive  $Y_e$  towards 0.5, disfavoring the  $r$ -process. *Right*: Electron neutrino and antineutrino luminosities ( $L_{\nu_e}$  and  $L_{\bar{\nu}_e}$  in units of  $10^{51}$  erg/s; upper panel) for our toy model (see text for details) as functions of the distance  $r$  from the center of the PNS, at  $t_0 = 2.9$  s, for “active” and “sterile” cases. Lower panel: Similar to the upper panel, but for the mean energies  $\langle E_{\nu_e} \rangle$  and  $\langle E_{\bar{\nu}_e} \rangle$ . (The red lines are running averages over  $\Delta r \approx 1.98 \cdot 10^5$  cm.)

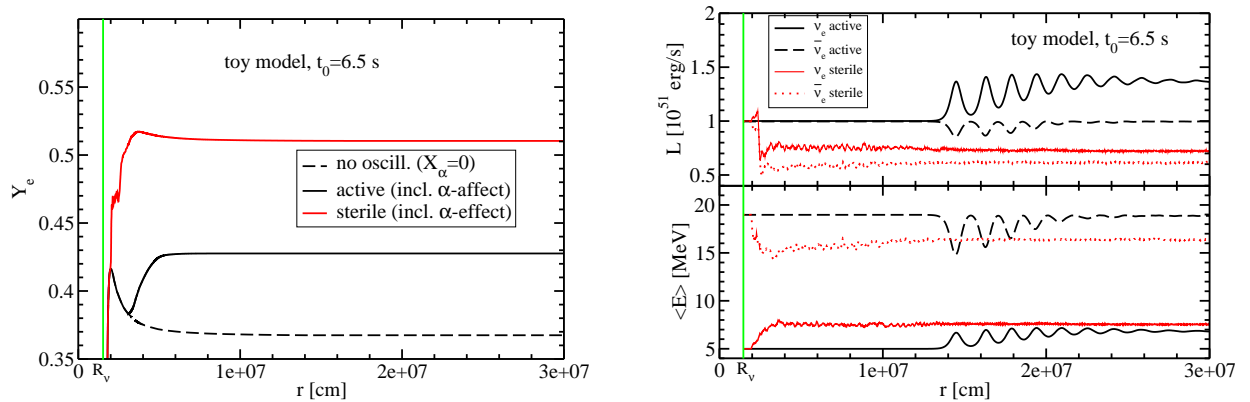


FIG. 8.— *Left*: Same as Fig. 7, but for the toy model at  $t_0 = 6.5$  s (see text for details). (The red lines here are running averages over  $\Delta r \approx 1.1 \cdot 10^5$  cm.)

however, recent works suggest that this might be valid only in the early ( $t_{\text{pb}} \lesssim 1$  s) and late ( $t_{\text{pb}} \gtrsim 3$  s) wind phases. Including mean-field nucleon potential corrections for the charged-current neutrino opacities in the dense medium of the proto-neutron star (Reddy et al. 1998) can cause  $Y_e$  of the wind material to become neutron-rich (possibly down to  $Y_e \simeq 0.42\text{--}0.45$ , Roberts 2012; Martínez-Pinedo et al. 2012; Roberts et al. 2012) during an intermediate evolution period, although the result is sensitively dependent on the employed nuclear equation of state. To explore the role of neutrino oscillations in such a neutron-rich environment, we construct four toy models to emulate the mean-field corrections of the neutrino opacities in their effect on lowering  $\langle E_{\nu_e} \rangle$  and increasing  $\langle E_{\bar{\nu}_e} \rangle$ .

In order to mimic the nucleon potential corrections, we select the intermediate  $t_0 = 2.9$  s and the late  $t_0 = 6.5$  s post-bounce times (see Table 1). We artificially prescribe the  $\nu_e$  and  $\bar{\nu}_e$  spectra by choosing the shape factors<sup>11</sup> corresponding to  $\alpha_{\nu_e} = \alpha_{\bar{\nu}_e} = 4$ . While leaving all the other neutrinospheric parameters, in particular the neutrino luminosities, unchanged as in Table 1, we set the values for the mean energies such that a neutron-rich environment results in the  $\nu$ -driven wind without oscillations (see first two cases in Table 2). We choose  $\langle E_{\nu_e} \rangle$  and  $\langle E_{\bar{\nu}_e} \rangle$  to obtain an asymptotic (indicated by the subscript “a”) electron fraction<sup>12</sup> including the  $\alpha$ -effect ( $Y_{e,a}$ ), or neglecting it ( $Y_{e,a}^{X_\alpha=0}$ ), lower than 0.5, as given in Table 2 (first two cases). We adopt the “artificial spectra” constructed in this way as initial conditions for the neutrino evolution. In Fig. 7 and in Fig. 8 (left panels), we show  $Y_e^{X_\alpha=0}$  as a function of the radius (black dashed lines). We also display  $Y_e$  radial profiles, including the  $\alpha$ -effect in the “active” (solid black lines) and “sterile” (solid red lines) cases.

In the “active” cases the asymptotic values of the electron fractions are  $Y_{e,a}^{\text{act}} \simeq 0.422$  and  $Y_{e,a}^{\text{act}} \simeq 0.428$  for  $t_0 = 2.9$  s and  $t_0 = 6.5$  s, respectively. Since “active” oscillations happen for  $r > 1.2 \times 10^7$  cm in both cases (i.e., after  $Y_e$  has reached its asymptotic value), the difference  $Y_{e,a}^{\text{act}} - Y_{e,a}^{X_\alpha=0} \simeq 0.02$  for  $t_0 = 2.9$  s ( $\simeq 0.06$ , for  $t_0 = 6.5$  s) is due to the  $\alpha$ -effect (see Table 2). Also for these toy models, in analogy to what we discussed in Sect. 5, the impact of the  $\alpha$ -effect on  $Y_e$  is larger at late times.

In the “sterile” case, oscillations rise the asymptotic value of the electron fraction to  $Y_{e,a}^{\text{ste}} \simeq 0.43$  (at  $t_0 = 2.9$  s) and to  $Y_{e,a}^{\text{ste}} \simeq 0.51$  (at  $t_0 = 6.5$  s). Therefore,  $Y_{e,a}^{\text{ste}} - Y_{e,a}^{X_\alpha=0}(2.9 \text{ s}) \simeq 0.03$  and  $Y_{e,a}^{\text{ste}} - Y_{e,a}^{X_\alpha=0}(6.5 \text{ s}) \simeq 0.14$ . This means that the matter becomes *more proton rich* compared to the case where oscillations are not considered or where they occur in the active sector only, since  $Y_{e,a}^{\text{ste}} - Y_{e,a}^{\text{act}} \simeq 0.01$  for  $t_0 = 2.9$  s and  $\simeq 0.08$  for  $t_0 = 6.5$  s (see Table 2).

The reason for  $Y_{e,a}^{\text{act,ste}} > Y_{e,a}^{X_\alpha=0}$  becomes clear from Fig. 7 and Fig. 8 (right panels), where we show the luminosities and mean energies of  $\nu_e$  and  $\bar{\nu}_e$  for the active and sterile cases as functions of the radius in order to better understand the influence of neutrino oscillations on  $Y_e$  via Eq. (4). In the “active” case, the different initial conditions (i.e.,  $L_{\nu_e}/\langle E_{\nu_e} \rangle - L_{\bar{\nu}_e}/\langle E_{\bar{\nu}_e} \rangle > 0$  for neutrinos, and the larger differences between the  $\nu_e$  ( $\bar{\nu}_e$ ) and  $\nu_x$  spectra and their spectral crossings)

trigger bipolar oscillations due to  $\nu$ - $\nu$  interactions (Fogli et al. 2008, 2009b) at  $R \simeq 2.2 \times 10^7$  cm for  $t_0 = 2.9$  s and  $R \simeq 1.35 \times 10^7$  cm for  $t_0 = 6.5$  s. This modifies the luminosities and the mean energies correspondingly, while  $X_\alpha$  and  $Y_e$  reach their asymptotic values at a smaller radius of about  $\simeq 10^7$  cm (see Fig. 7 and Fig. 8). Therefore, for both post-bounce times, neutrino oscillations in the active sector start only when  $Y_e$  has already reached its asymptotic value and thus flavor oscillations have no influence on  $Y_e$ . However, for the reasons explained above, neutrino oscillations in the “active” case have a non-negligible impact on the neutrino properties in our toy models. This is different from the previously considered “active” cases where the un-oscillated neutrino fluxes were very similar and no significant variations in the integrated neutrino properties due to collective oscillations were visible (see Fig. 3 and Fig. 4 for comparison).

An interesting complication appears for sterile neutrino oscillations in both toy models, because  $Y_e$  is lower than in the standard cases and the energy spectra of  $\nu_e$  and  $\bar{\nu}_e$  have very different mean energies and are significantly different from those of the heavy-lepton flavors. Therefore, an interplay between  $\alpha$ -effect, neutrino self-interactions and inner/outer MSW resonances may occur due to the overlap of the spatial regions where these effects take place. For investigating the consequences, we include the inner MSW resonance in our numerical computations.

As shown in Fig. 7 for  $t_0 = 2.9$  s (right panel), the inner resonance, close to the neutrinosphere, converts both  $\nu_e$  and  $\bar{\nu}_e$  to sterile states. Due to the feedback effect of oscillations on  $Y_e$  and due to the lower value of  $Y_e$  compared to the corresponding standard case, the outer MSW resonance is more adiabatic and occurs at smaller radii ( $r \simeq 3 \cdot 10^6$  cm) than in the standard case (see Fig. 3), almost overlapping with the inner resonance region and partly repopulating the  $\nu_e$  flux, as can be seen by the increase of  $L_{\nu_e}/\langle E_{\nu_e} \rangle$  (the same happens to antineutrinos, although less significantly). Due to the hierarchy of the active neutrino fluxes and due to the lower matter potential, collective oscillations strongly mix  $\nu_e$  and  $\bar{\nu}_e$  with the heavy lepton flavors. Correspondingly,  $Y_e$  (left panel, Fig. 7) first decreases compared to the cases without sterile neutrinos close to the neutrinosphere and then it rises again thanks to the interplay of the outer resonance and collective oscillations, which increase  $L_{\nu_e}/\langle E_{\nu_e} \rangle$  and also, but less,  $L_{\bar{\nu}_e}/\langle E_{\bar{\nu}_e} \rangle$ . At  $r \simeq 4 \cdot 10^6$  cm, the  $Y_e$  growth is then mostly driven by the  $\alpha$ -effect (see for comparison the black solid and dashed curves of the left panel in Fig. 7). Notice that this toy model differs from the standard  $t_0 = 2.9$  s case discussed in Sect. 5, making it a pretty peculiar case of study for three reasons: First,  $Y_e \simeq 1/3$  in a wider spatial region closer to the neutrinosphere, resembling the  $Y_e$  behavior during the accretion phase and therefore making the inner resonance non-negligible (similar to what was discussed in Wu et al. 2014). Secondly, the outer resonance is more adiabatic because of the feedback effect and it almost overlaps spatially with the inner resonance. Thirdly, collective oscillations play a larger role, given the hierarchy of the active fluxes (compare the red and black lines in Fig. 7).

We point out that in the sterile case  $Y_e$  does not increase as much as expected from the increase of the  $\nu_e$  number flux (see Fig. 7, right panel), because collective oscillations overlap with the region where  $\alpha$  particles start forming, which remove free nucleons and thus moderate the impact of neutrino oscillations on  $Y_e$ , as discussed in detail in Sect. 5. In particular, for intermediate evolution phases of the  $\nu$ -driven wind,

<sup>11</sup> We assume the shape factors of a moderately degenerate Fermi-Dirac distribution, for which  $\langle E_\nu^2 \rangle / \langle E_\nu \rangle^2 \simeq 1.2$  (Horowitz & Li 1999).

<sup>12</sup> Note that Roberts et al. (2012) employed the approximative formula  $Y_e \simeq 1/(1 + \lambda_{\bar{\nu}_e}/\lambda_{\nu_e})$  of Qian & Fuller (1995) for estimating the electron fraction in the wind. This formula does not account for the  $\alpha$ -effect on  $Y_e$ .

despite the presence of sterile neutrinos, the environment remains still neutron-rich, although even *less neutron-rich* than in the cases without sterile neutrinos.

At  $t_0 = 6.5$  s, the MSW inner resonance plays an almost negligible role in the “sterile” case (see Fig. 8), similar to the situation in the standard cases. The presence of such a resonance is visible by a small decrease of  $L_{\nu_e}/\langle E_{\nu_e} \rangle$  (and even smaller for the  $\bar{\nu}_e$ ) at  $r \approx 2 \cdot 10^6$  cm. Slightly farther outside, at  $r \approx 2.5 \cdot 10^6$  cm, the outer MSW resonance occurs (similarly to the standard case). Sterile neutrinos and antineutrinos are both abundantly produced through flavor conversions due to an interplay between the outer MSW resonance and collective oscillations, before  $\alpha$  particles start forming at  $r \approx 3 \cdot 10^6$  cm.

As a consequence, both  $\nu_e$  and  $\bar{\nu}_e$  fluxes decrease, causing an increase of  $Y_e$  above 0.5 before the onset of the  $\alpha$ -effect, which reduces  $Y_e$  slightly again at  $r \gtrsim 3 \cdot 10^6$  cm, producing an asymptotic value of  $Y_e \approx 0.51$ .

Since the  $\bar{\nu}_e$  luminosity in the “sterile” case varies more than the  $\nu_e$  luminosity, whereas the mean energy of  $\bar{\nu}_e$  experiences a relatively moderate change only (Fig. 8, right panel),  $\bar{\nu}_e$  captures on free protons are more significantly reduced than  $\nu_e$  captures on free neutrons (Eqs. 2,3). This results in a more abundant proton production in the wind, i.e.  $Y_e$  becomes higher in the presence of sterile neutrinos. This is again a consequence of the interplay of  $\nu$ - $\nu$  interactions, active-sterile MSW resonances and  $\alpha$ -effect.

In our toy models, we assume the neutrinospheric  $\nu_e$  and  $\bar{\nu}_e$  luminosities as given in Table 1. However, luminosities and mean energies both affect  $Y_e$  at the same time through the rates in Eq. (4). In order to prove the robustness of our results, we consider two more test cases, now keeping the neutrinospheric number fluxes (i.e. the  $L_\nu/\langle E_\nu \rangle$  ratios) fixed as given by the hydrodynamic simulations for  $t_0 = 2.9$  s and  $t_0 = 6.5$  s and varying both luminosities and mean energies of  $\nu_e$  and  $\bar{\nu}_e$  in order to obtain  $Y_{e,a}^{X_\alpha=0} \approx 0.405$  and  $0.380$  for  $t_0 = 2.9$  s and  $t_0 = 6.5$  s, respectively (see the third and fourth cases in Table 2). Also in these cases the observed trend is reproduced: Neutrino oscillations in the presence of a sterile state together with the  $\alpha$ -effect rise the asymptotic  $Y_e$  by about 0.04 and 0.11 for  $t_0 = 2.9$  s and  $t_0 = 6.5$  s, respectively, compared to  $Y_{e,a}^{X_\alpha=0}$ .

In conclusion, neutrino oscillations (with or without sterile neutrinos) combined with the  $\alpha$ -effect do not support very neutron-rich conditions in the neutrino-driven wind for the considered SN model. Therefore, conditions for a strong r-process in this SN progenitor are disfavored, because  $Y_e$  tends to be pushed close to 0.5 and thus the formation of a highly neutron-rich environment is prevented.

## 7. CONCLUSIONS

We presented neutrino oscillations and nucleosynthesis calculations for the neutrino-cooling phase of the proto-neutron star born in an  $8.8 M_\odot$  electron-capture supernova, using trajectories for the  $\nu$ -driven wind from 1D hydrodynamic simulations, in which a sophisticated treatment of neutrino transport was applied (Hühdepohl et al. 2010). In particular, we studied the consequences of neutrino oscillations of two active flavors driven by the atmospheric mass difference and  $\theta_{13}$  and, motivated by recent hints on the possible existence of light sterile neutrinos, we also discussed the role of flavor oscillations with 1 sterile + 2 active flavors. In our study neutrino-neutrino refraction effects were included, too. We chose  $\nu_e$ - $\nu_s$  mixing parameters as suggested by the reactor anomaly (Mention et al. 2011). However, our conclusions re-

main valid also for moderate variations of the sterile mass-mixing parameters.

As found in Tamborra et al. (2012b), neutrino conversions to a sterile flavor and collective transformations of active flavors influence the radial variation and time-dependent asymptotic value of  $Y_e$  in the neutrino-driven wind in complicated ways. (MSW oscillations in the active sector occur at too large radii to be of any relevance in this context.) The feedback of active-sterile oscillations on neutrino-refractive effects causes intriguing nonlinear modifications of the naive oscillation picture, and the active-active oscillations can play an important additional role in determining the neutron-to-proton ratio of the SN ejecta. These conclusions motivated us to investigate in detail the effect of oscillations on a larger variety of wind conditions and on the nucleosynthetic abundances. Different from Tamborra et al. (2012b) the  $\alpha$ -effect on the  $Y_e$  evolution is fully accounted for, and recoil and weak magnetism corrections are included in the  $\beta$  processes as well.

Our results demonstrate that the  $\alpha$ -effect plays a crucial role in discussing the consequences of neutrino oscillations on the  $Y_e$  evolution in neutrino-driven winds. It can damp as well as enhance the  $Y_e$ -reducing impact of  $\nu_e$ - $\nu_s$  conversions, depending on the radial position of the active-sterile MSW region relative to the radius where  $\alpha$ -particles form from nucleon recombination. In the late proto-neutron star cooling phase the production of sterile neutrinos via an MSW resonance takes place very close to the neutrinosphere, while a significant abundance of  $\alpha$ -particles in the wind appears only at larger distances. The  $Y_e$  reduction in the ejecta associated with the transformation of  $\nu_e$  to  $\nu_s$  is therefore amplified by the subsequent  $\alpha$ -effect, driving  $Y_e$  from initial values considerably above 0.5 to an asymptotic value closer to 0.5. In the early wind phase the effect is different. Here the outer  $\nu_e$ - $\nu_s$  MSW conversions occur farther away from the neutron star and exterior to (or coincident with) the formation region of  $\alpha$ -particles. The  $\alpha$ -effect then moderates the  $Y_e$  reduction caused by the presence of sterile neutrinos. Because of this dominance of the  $\alpha$ -effect, the asymptotic neutron-to-proton ratio in the early wind becomes very similar for the cases with and without sterile neutrinos (whereas without  $\alpha$ -effect sterile neutrinos always cause a significant reduction of  $Y_e$ ).

While the neutrino-driven wind of our ECSN model is well on the proton-rich side (Hühdepohl et al. 2010), equation-of-state dependent nucleon mean-field potentials in the neutrinospheric region might lead to a considerably lower  $Y_e$  in the wind outflow (Roberts et al. 2012; Martínez-Pinedo et al. 2011). For this reason we constructed four toy model cases for the intermediate and late wind phases, in which the (unoscillated) neutrino spectra were chosen such that the neutrino-driven wind became neutron-rich with an asymptotic wind- $Y_e$  (including the  $\alpha$ -effect) of about 0.42–0.43, which is on the extreme side of the theoretical estimates. Including active-sterile flavor oscillations, the outflow turns *more proton-rich*, despite the conversion of  $\nu_e$  to  $\nu_s$ . This counterintuitive  $Y_e$  increase is caused by neutrino oscillations, which modify the neutrino emission properties such that either the  $\nu_e$  absorption is more strongly increased than the competing  $\bar{\nu}_e$  absorption or the  $\bar{\nu}_e$  absorption is more strongly reduced than the competing  $\nu_e$  absorption. Our conclusion that sterile neutrinos are unlikely to help enforcing neutron-rich conditions in the wind ejecta therefore seems to remain valid even when nucleon-potential effects are taken into account in future neutron-star cooling simulations.

If oscillations are disregarded, the wind ejecta in our ECSN

model develop a proton excess and therefore only iron-group and some  $p$ -rich isotopes are created with small production factors (below 10), not adding any significant production of interesting isotopes to the nucleosynthesis yields computed for the early ejecta of 2D explosion models of such EC-SNe (Wanajo et al. 2011b, 2013a,b). When neutrino oscillations are taken into account by our simplified neutrino-mixing scheme, the feedback of oscillations on  $Y_e$  is time-dependent, since it is sensitive to the detailed matter profile and neutrino fluxes. In the early  $\nu$ -driven wind, the asymptotic  $Y_e$  value in the presence of a sterile family is almost the same as the  $Y_e$  value obtained without oscillations. In contrast, in the late  $\nu$ -driven wind the asymptotic  $Y_e$  in the presence of sterile neutrinos is slightly lowered compared to the case without oscillations or to the case where oscillations in the active sector are considered. However, in our model of the neutrino cooling of the proto-neutron star born in an ECSN, the corresponding effects do not lead to any neutron excess. The changes of the nucleosynthetic output for models with (active or sterile) neutrino oscillations compared to the no oscillations case are insignificant. It appears unlikely that in the studied progenitor viable conditions for strong r-processing can be established.

Like all other numerical studies of neutrino oscillations with neutrino-neutrino refraction, we made simplifying assumptions to cope with the complex, nonlinear nature of the problem. In our case, we averaged the angular dependence of  $\nu$ - $\nu$  interactions (Duan et al. 2006) because of the numerical complications induced by the  $Y_e$  feedback on neutrino oscillations and vice versa. Although first more sophisticated “multi-angle studies” have investigated the role of the full multi-angle dependence of neutrino interactions and have abolished the assumption of axial symmetry around the radial direction (see Raffelt et al. 2013; Mirizzi 2013a,b), these studies still involve a number of approximations. A fully general numerical treatment is not yet available. Because of the

similarity between the  $\nu_e$  and  $\bar{\nu}_e$  fluxes and those of the heavy-lepton neutrinos in our simulations with only active-flavor oscillations, and the observed strength of the  $\alpha$ -effect in pushing  $Y_e$  close to 0.5, even a possible relevance of multi-angle effects (Esteban-Pretel et al. 2007) is unlikely to have important consequences for  $Y_e$ . For the same reasons we do not expect that effects emerging from a full multi-angle treatment in the case of a normal mass-hierarchy in the active sector ( $\delta m_{\text{atm}}^2 > 0$ ) will lead to conditions that allow for strong r-processing.

Our conclusions concern the  $\nu$ -driven wind of an  $8.8 M_{\odot}$  progenitor. More studies of the impact of neutrino oscillations on the early-time ejecta including multi-dimensional effects arising in hydrodynamic simulations (Wanajo et al. 2011b, 2013a) and including the effects of nucleon mean-field potentials in the neutrino opacities, are needed in order to shed light on the consequences of neutrino oscillations for the explosion mechanism and nucleosynthetic abundances (cf. Wu et al. 2014, who considered only a 1D model). Studies of a broader range of progenitor models, in particular also iron-core SNe with more massive proto-neutron stars, applying state-of-the-art neutrino-oscillation physics, are also desirable to identify possible cases where favorable conditions for an r-process may be produced.

#### ACKNOWLEDGEMENTS

E.P. is thankful to Bernhard Müller for useful discussions. I.T. acknowledges support from the Netherlands Organization for Scientific Research (NWO). S.W. acknowledges partial support from the RIKEN iTHES Project and the JSPS Grants-in-Aid for Scientific Research (26400232, 26400237). Partial support from the Deutsche Forschungsgemeinschaft through the Transregional Collaborative Research Center SFB/TR 7 “Gravitational Wave Astronomy” and the Cluster of Excellence EXC 153 “Origin and Structure of the Universe” (<http://www.universe-cluster.de>) is also acknowledged.

#### REFERENCES

- Abazajian, K. N., et al. 2012, arXiv:1204.5379  
Aguilar, A., et al. 2001, *Phys. Rev. D*, 64, 112007  
Aguilar-Arevalo, A. A., et al. 2009a, *Phys. Rev. Lett.*, 103, 111801  
—, 2009b, *Phys. Rev. Lett.*, 102, 101802  
Archidiacono, M., Fornengo, N., Giunti, C., Hannestad, S., & Melchiorri, A. 2013, *Phys. Rev. D*, 87, 125034  
Arcones, A., & Montes, F. 2011, *ApJ*, 731, 5  
Arcones, A., & Thielemann, F.-K. 2013, *Journal of Physics G Nuclear Physics*, 40, 013201  
Arnould, M., Goriely, S., & Takahashi, K. 2007, *Phys. Rep.*, 450, 97  
Aver, E., Olive, K. A., & Skillman, E. D. 2012, *JCAP*, 4, 4  
Beun, J., McLaughlin, G. C., Surman, R., & Hix, W. R. 2006, *Phys. Rev. D*, 73, 093007  
Bruenn, S. W. 1985, *ApJS*, 58, 771  
Capozzi, F., Fogli, G. L., Lisi, E., Marrone, A., Montanino, D., & Palazzo, A. 2013, ArXiv e-prints:1312.2878  
Chakraborty, S., Fischer, T., Mirizzi, A., Saviano, N., & Tomàs, R. 2011, *Phys. Rev. Lett.*, 107, 151101  
Dasgupta, B., & Dighe, A. 2008, *Phys. Rev. D*, 77, 113002  
Dasgupta, B., Mirizzi, A., Tamborra, I., & Tomàs, R. 2010, *Phys. Rev. D*, 81, 093008  
Donini, A., Hernández, P., López-Pavón, J., Maltoni, M., & Schwetz, T. 2012, *Journal of High Energy Physics*, 7, 161  
Duan, H., Friedland, A., McLaughlin, G. C., & Surman, R. 2011, *Journal of Physics G Nuclear Physics*, 38, 035201  
Duan, H., Fuller, G. M., Carlson, J., & Qian, Y.-Z. 2006, *Phys. Rev. D*, 74, 105014  
Duan, H., Fuller, G. M., & Qian, Y.-Z. 2010, *Annual Review of Nuclear and Particle Science*, 60, 569  
Esteban-Pretel, A., Pastor, S., Tomàs, R., Raffelt, G. G., & Sigl, G. 2007, *Phys. Rev. D*, 76, 125018  
Fetter, J., McLaughlin, G. C., Balantekin, A. B., & Fuller, G. M. 2003, *Astroparticle Physics*, 18, 433  
Fetter, J. M. 2000, PhD thesis, The University of Wisconsin – Madison  
Fischer, T., Martínez-Pinedo, G., Hempel, M., & Liebendörfer, M. 2012, *Phys. Rev. D*, 85, 083003  
Fischer, T., Whitehouse, S. C., Mezzacappa, A., Thielemann, F.-K., & Liebendörfer, M. 2010, *A&A*, 517, A80  
Fogli, G., Lisi, E., Marrone, A., & Mirizzi, A. 2007, *JCAP*, 12, 10  
Fogli, G., Lisi, E., Marrone, A., & Tamborra, I. 2009a, *JCAP*, 4, 30  
—, 2009b, *JCAP*, 10, 2  
Fogli, G. L., Lisi, E., Marrone, A., Mirizzi, A., & Tamborra, I. 2008, *Phys. Rev. D*, 78, 097301  
Fogli, G. L., Lisi, E., Marrone, A., & Palazzo, A. 2006, *Progress in Particle and Nuclear Physics*, 57, 742  
Fröhlich, C., Martínez-Pinedo, G., Liebendörfer, M., Thielemann, F.-K., Bravo, E., Hix, W. R., Langanke, K., & Zinner, N. T. 2006a, *Phys. Rev. Lett.*, 96, 142502  
Fröhlich, C., et al. 2006b, *ApJ*, 637, 415  
Fuller, G. M., & Meyer, B. S. 1995, *ApJ*, 453, 792  
Giunti, C., & Laveder, M. 2011a, *Physics Letters B*, 706, 200  
—, 2011b, *Phys. Rev. D*, 84, 093006  
Giunti, C., Laveder, M., Li, Y. F., Liu, Q. Y., & Long, H. W. 2012, *Phys. Rev. D*, 86, 113014  
Giunti, C., Laveder, M., Li, Y. F., & Long, H. W. 2013, *Phys. Rev. D*, 88, 073008  
Giusarma, E., Di Valentino, E., Lattanzi, M., Melchiorri, A., & Mena, O. 2014, ArXiv e-prints:1403.4852  
Gonzalez-Garcia, M. C., & Maltoni, M. 2008, *Phys. Rep.*, 460, 1

- Hamann, J., Hannestad, S., Raffelt, G. G., Tamborra, I., & Wong, Y. Y. Y. 2010, *Phys. Rev. Lett.*, 105, 181301
- Hannestad, S., Raffelt, G. G., Sigl, G., & Wong, Y. Y. Y. 2006, *Phys. Rev. D*, 74, 105010
- Hidaka, J., & Fuller, G. M. 2007, *Phys. Rev. D*, 76, 083516
- Hillebrandt, W., Nomoto, K., & Wolf, R. G. 1984, *A&A*, 133, 175
- Hinshaw, G., et al. 2013, *ApJS*, 208, 19
- Hoffman, R. D., Müller, B., & Janka, H.-T. 2008, *ApJ*, 676, L127
- Hoffman, R. D., Woosley, S. E., & Qian, Y.-Z. 1997, *ApJ*, 482, 951
- Horowitz, C. J., & Li, G. 1999, *Phys. Rev. Lett.*, 82, 5198
- Hou, Z., Keisler, R., Knox, L., Millea, M., & Reichardt, C. 2013, *Phys. Rev. D*, 87, 083008
- Hüdepohl, L., Müller, B., Janka, H.-T., Marek, A., & Raffelt, G. G. 2010, *Phys. Rev. Lett.*, 104, 251101
- Ishimaru, Y., & Wanajo, S. 1999, *ApJ*, 511, L33
- Janka, H.-T. 2012, *Annual Review of Nuclear and Particle Science*, 62, 407
- Janka, H.-T., Müller, B., Kitaura, F. S., & Buras, R. 2008, *A&A*, 485, 199
- Karagiorgi, G., Djuricic, Z., Conrad, J. M., Shaevitz, M. H., & Sorel, M. 2009, *Phys. Rev. D*, 80, 073001
- Keil, M. T., Raffelt, G. G., & Janka, H.-T. 2003, *ApJ*, 590, 971
- Keränen, P., Maalampi, J., Myrskyläinen, M., & Riittinen, J. 2007, *Phys. Rev. D*, 76, 125026
- Kitaura, F. S., Janka, H.-T., & Hillebrandt, W. 2006, *A&A*, 450, 345
- Kopp, J., Maltoni, M., & Schwetz, T. 2011, *Phys. Rev. Lett.*, 107, 091801
- Lodders, K. 2003, *ApJ*, 591, 1220
- Martínez-Pinedo, G., Fischer, T., Lohs, A., & Huther, L. 2012, *Phys. Rev. Lett.*, 109, 251104
- Martínez-Pinedo, G., Ziebarth, B., Fischer, T., & Langanke, K. 2011, *European Physical Journal A*, 47, 98
- McLaughlin, G. C., Fetter, J. M., Balantekin, A. B., & Fuller, G. M. 1999, *Phys. Rev. C*, 59, 2873
- McLaughlin, G. C., Fuller, G. M., & Wilson, J. R. 1996, *ApJ*, 472, 440
- Mention, G., Fechner, M., Lasserre, T., Mueller, T. A., Lhuillier, D., Cribier, M., & Letourneau, A. 2011, *Phys. Rev. D*, 83, 073006
- Meyer, B. S., Mathews, G. J., Howard, W. M., Woosley, S. E., & Hoffman, R. D. 1992, *ApJ*, 399, 656
- Meyer, B. S., McLaughlin, G. C., & Fuller, G. M. 1998, *Phys. Rev. C*, 58, 3696
- Mikheyev, S. P., & Smirnov, A. Y. 1985, *Yadernaya Fizika*, 42, 1441
- MiniBooNE Collaboration et al. 2012, *arXiv:1207.4809*
- Mirizzi, A. 2013a, *Phys. Rev. D*, 88, 073004
- 2013b, *ArXiv e-prints:1308.5255*
- Ning, H., Qian, Y.-Z., & Meyer, B. S. 2007, *ApJ*, 667, L159
- Nomoto, K. 1987, *ApJ*, 322, 206
- Nunokawa, H., Peltoniemi, J. T., Rossi, A., & Valle, J. W. F. 1997, *Phys. Rev. D*, 56, 1704
- Otsuki, K., Tagoshi, H., Kajino, T., & Wanajo, S.-y. 2000, *ApJ*, 533, 424
- Palazzo, A. 2013, *Modern Physics Letters A*, 28, 30004
- Pettini, M., & Cooke, R. 2012, *MNRAS*, 425, 2477
- Planck Collaboration et al. 2013, *arXiv:1303.5076*
- Poelarends, A. J. T., Herwig, F., Langer, N., & Heger, A. 2008, *ApJ*, 675, 614
- Pruet, J., Hoffman, R. D., Woosley, S. E., Janka, H.-T., & Buras, R. 2006, *ApJ*, 644, 1028
- Qian, Y.-Z., & Fuller, G. M. 1995, *Phys. Rev. D*, 52, 656
- Qian, Y.-Z., & Woosley, S. E. 1996, *ApJ*, 471, 331
- Raffelt, G., Sarikas, S., & Seixas, D. d. S. 2013, *Phys. Rev. Lett.*, 111, 091101
- Reddy, S., Prakash, M., & Lattimer, J. M. 1998, *Phys. Rev. D*, 58, 013009
- Reid, B. A., Verde, L., Jimenez, R., & Mena, O. 2010, *JCAP*, 1, 3
- Roberts, L. F. 2012, *ApJ*, 755, 126
- Roberts, L. F., Reddy, S., & Shen, G. 2012, *Phys. Rev. C*, 86, 065803
- Sarikas, S., Raffelt, G. G., Hüdepohl, L., & Janka, H.-T. 2012, *Phys. Rev. Lett.*, 108, 061101
- Shen, H., Toki, H., Oyamatsu, K., & Sumiyoshi, K. 1998, *Nuclear Physics A*, 637, 435
- Sigl, G., & Raffelt, G. 1993, *Nuclear Physics B*, 406, 423
- Strumia, A. 2002, *Physics Letters B*, 539, 91
- Takahashi, K., Wittl, J., & Janka, H.-T. 1994, *A&A*, 286, 857
- Tamborra, I., Müller, B., Hüdepohl, L., Janka, H.-T., & Raffelt, G. 2012a, *Phys. Rev. D*, 86, 125031
- Tamborra, I., Raffelt, G. G., Hüdepohl, L., & Janka, H.-T. 2012b, *JCAP*, 1, 13
- Thielemann, F.-K., et al. 2011, *Progress in Particle and Nuclear Physics*, 66, 346
- Thompson, T. A., Burrows, A., & Meyer, B. S. 2001, *ApJ*, 562, 887
- Wanajo, S. 2006, *ApJ*, 647, 1323
- Wanajo, S., & Ishimaru, Y. 2006, *Nuclear Physics A*, 777, 676
- Wanajo, S., Janka, H.-T., & Kubono, S. 2011a, *ApJ*, 729, 46
- Wanajo, S., Janka, H.-T., & Müller, B. 2011b, *ApJ*, 726, L15
- 2013a, *ApJ*, 767, L26
- 2013b, *ApJ*, 774, L6
- Wanajo, S., Kajino, T., Mathews, G. J., & Otsuki, K. 2001, *ApJ*, 554, 578
- Wanajo, S., Nomoto, K., Janka, H.-T., Kitaura, F. S., & Müller, B. 2009, *ApJ*, 695, 208
- Wanajo, S., Tamamura, M., Itoh, N., Nomoto, K., Ishimaru, Y., Beers, T. C., & Nozawa, S. 2003, *ApJ*, 593, 968
- Wolfenstein, L. 1978, *Phys. Rev. D*, 17, 2369
- Woosley, S. E., Heger, A., & Weaver, T. A. 2002, *Rev. Mod. Phys.*, 74, 1015
- Woosley, S. E., Wilson, J. R., Mathews, G. J., Hoffman, R. D., & Meyer, B. S. 1994, *ApJ*, 433, 229
- Wu, M.-R., Fischer, T., Huther, L., Martínez-Pinedo, G., & Qian, Y.-Z. 2014, *Phys. Rev. D*, 89, 061303